Geoderma 465 (2026) 117648

Contents lists available at ScienceDirect

Geoderma

journal homepage: www.elsevier.com/locate/geoderma

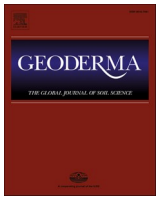

Short-term effects of harvesting alternatives on soil nitrous oxide fluxes in a boreal drained peatland forest

Eduardo Martínez-García [a,*], Helena Rautakoski [b], Antti J. Rissanen [c,a], Bartosz Adamczyk [a], Jani Anttila [a], Aleksi Lehtonen [a], Qian Li [a], Annalea Lohila [b,d], Mikko Peltoniemi [a], Sakari Sarkkola [a], Boris Ťupek [a], Raisa Mäkipää [a]

[a] Natural Resources Institute Finland (Luke), Latokartanonkaari 9, FI-00790 Helsinki, Finland
[b] Finnish Meteorological Institute (FMI), Erik Palménin aukio 1, FI-00560 Helsinki, Finland
[c] Faculty of Engineering and Natural Sciences, Tampere University, Korkeakoulunkatu 6, FI-33720 Tampere, Finland
[d] Institute for Atmospheric and Earth System Research (INAR)/Physics, University of Helsinki, Gustaf Hällströmin katu 2, FI-00014 Helsinki, Finland

ARTICLE INFO

Handling Editor: Dr Daniel Said-Pullicino

Keywords:
N_2O
Clear-cutting
Continuous-cover forestry
Selection harvesting
Temporal variation
Spatial variation

ABSTRACT

Extensive areas of boreal peatland forests in the Nordic countries are approaching maturity and face harvesting, yet effects on soil nitrous oxide (N_2O) fluxes remain unclear. This study examined short-term changes in soil N_2O fluxes following two harvesting methods, clear-cutting (CC) and continuous-cover forestry via selection harvesting (CCF), compared to a non-harvested control (C) in a nutrient-rich, forestry-drained boreal peatland in southern Finland. Fluxes were measured using manual and automated chambers during pre-harvest (2020) and post-harvest (2021–2022) periods, alongside soil physical, chemical, and environmental properties to identify key controls of flux variability.

N_2O fluxes showed high temporal variation (−39 to 459 μg N_2O m^{-2} h^{-1}), primarily driven by temperature, precipitation, moisture, and water table dynamics, and pronounced spatial variation linked to soil nutrient concentrations (potassium, copper, phosphorus, and nitrogen), bulk density, and temperature. While emissions remained near neutral at the C site, harvesting increased emissions, although not significantly. In the first post-harvest year, annual emissions increased with harvesting intensity, yet no significant differences emerged between CCF and CC. Median [interquartile range] emissions were 0 [25], 163 [533], and 185 [194] mg N_2O m^{-2} y^{-1} at the C, CCF and CC sites, respectively, with inherent spatial variability strongly influencing their spatial distribution. Limited water table rise at the CCF site and high spatial heterogeneity at the CC site likely constrained clearer treatment differences. Overall, our findings suggest that CCF may better mitigate emissions than CC in nutrient-rich, forestry-drained boreal peatlands, warranting further replicated and long-term research.

1. Introduction

The atmospheric concentration of nitrous oxide (N_2O) has increased by ~24.4 %, from 270 parts per billion (ppb) in pre-industrial times (1750) to 333 ppb in 2020, with an average annual increase of 0.96 ppb during 2010–2019 (Tian et al., 2024). As a long-lived and potent greenhouse gas (GHG), N_2O accounts for ~10 % of global radiative forcing (Forster et al., 2021) and is the primary stratospheric ozone-layer depleting substance (Ravishankara et al., 2009), prompting global interest in constraining its sources.

Bottom-up estimates of global N_2O emissions reached 18.2 Tg N y^{-1} (range: 10.6–25.9) over 2010–2019, with ~35 % from soils (Tian et al., 2024). Soil N_2O emissions primarily arise from two microbial processes: i) nitrification, the aerobic oxidation of ammonium (NH_4^+) to nitrate (NO_3^-), producing N_2O as a side product, and ii) denitrification, the anaerobic reduction of NO_3^- to N_2O or dinitrogen (N_2) (Regina et al., 1996). Soils may also act as temporary N_2O sinks (Chapuis-Lardy et al., 2007). Forest soils contribute significantly, releasing 3.0–4.5 Tg N y^{-1} (Cen et al., 2024), following a latitudinal gradient influenced by hydroclimate (Liao et al., 2024), with the highest fluxes in tropical forests (1.24 ± 0.24 Tg N y^{-1}, mean ± standard error), followed by temperate (0.78 ± 0.16 Tg N y^{-1}) and boreal forests (0.71 ± 0.14 Tg N y^{-1}; Cen et al. (2024)).

Boreal forests, covering ~27 % of global forest area (Pan et al.,

* Corresponding author.
E-mail address: eduardo.martinezgarcia@luke.fi (E. Martínez-García).

https://doi.org/10.1016/j.geoderma.2025.117648
Received 29 July 2025; Received in revised form 3 December 2025; Accepted 8 December 2025
Available online 12 December 2025

2011), comprise uplands, peatlands, and inland waters (~80 %, 15 %, and 5 %, respectively; Helbig et al., 2020). Despite their smaller area, peatlands play a major role in nitrogen (N) cycling and N_2O emissions due to high organic matter and waterlogged conditions. In their natural state, boreal peatlands are negligible N_2O sources or weak sinks (–5 to 207 mg N_2O m^{-2} y^{-1}; Minkkinen et al. (2020)), primarily due to limited oxygen (O_2) and nutrient availability under shallow water table level (WTL) conditions, which restrict microbial activity (Minkkinen et al., 2020; Regina et al., 1996). Drainage for forestry significantly alters these dynamics. Lowering the WTL increases O_2 availability, promoting nitrification, and often turning boreal peatlands into N_2O sources (Minkkinen et al., 2020; Pärn et al., 2018). Emissions from drained sites range from 37 to 1142 mg N_2O m^{-2} y^{-1} (Minkkinen et al., 2020). While N availability has minimal influence in natural boreal peatlands, N-rich drained sites emit more N_2O (203 ± 40 mg N_2O m^{-2} y^{-1}, mean ± standard error) than N-poor ones (80 ± 30 mg N_2O m^{-2} y^{-1}; Minkkinen et al. (2020)). Consequently, climate change mitigation efforts increasingly target forestry-drained boreal peatlands for rewetting, restoration, or improved forest management (Laine et al., 2024), highlighting the need for research to support low-emission strategies.

From the 1950 to early 1980s, ~9.5 million hectares of peatland were drained for forestry in the Nordic countries and Russia, with Finland accounting for 49 % (UNEP, 2022). While this increased timber production (Sikström and Hökkä, 2015), many drained peatland forests are now mature and approaching harvest (Lehtonen et al., 2023), which can significantly alter soil conditions regulating soil N_2O fluxes (Mäkipää et al., 2023; Zhang et al., 2022b). Yet, debate persists over which harvesting methods best minimize emissions from these managed peatlands (Lehtonen et al., 2023; Nieminen et al., 2018). Closing this knowledge gap is essential for developing climate-smart forest management in boreal regions.

Currently, clear-cutting-based rotation forestry (CC) is predominant in boreal drained peatlands (Härkönen et al., 2023). It involves harvesting most trees at once, creating even-aged stands typically dominated by a single tree species (Kuuluvainen et al., 2012). This method is increasingly scrutinized for adverse impacts on several ecosystem services (Nieminen et al., 2018). Continuous-cover-based forestry (CCF) has recently emerged as a potential alternative, maintaining uneven-aged stands through selection harvesting at 15–20-year intervals with natural regeneration (Rautio et al., 2025). Besides avoiding costs for site preparation, artificial regeneration, and ditch maintenance (Nieminen et al., 2018), CCF may reduce nutrient leaching and soil carbon dioxide (CO_2) emissions (Lehtonen et al., 2023).

Clear-cutting generally causes more intense and widespread soil disturbance than continuous-cover forestry. This includes: i) greater increases in soil water content and WTL due to reduced transpiration and canopy interception (Korkiakoski et al., 2019; Leppä et al., 2020; Sarkkola et al., 2010), ii) elevated soil temperature from increased solar exposure (Korkiakoski et al., 2019), iii) increased snow accumulation due to reduced canopy (Schelker et al., 2013), iv) higher soil bulk density from compaction across a larger disturbed areas (Lepilin et al., 2019), and v) greater carbon (C) and N inputs from more abundant logging residues (Mäkiranta et al., 2012). These impacts can persist for years or even decades (Lepilin, 2023). In contrast, selection harvesting in CCF, despite shorter treatment intervals, tends to produce less intense soil disturbance (Laudon and Maher Hasselquist, 2023). Thus, prolonged and intense changes after clear-cutting may lead to higher N_2O emissions than those resulting from the less disruptive selection harvesting. Although previous research suggests that CCF may result in lower short-term soil N_2O emissions than CC in forestry-drained boreal peatlands (Korkiakoski et al., 2020, Korkiakoski et al., 2019), comprehensive post-harvest assessments remain scarce, limiting our knowledge of soil N_2O dynamics in these forest ecosystems.

Understanding soil N_2O fluxes in boreal drained peatland forests is further complicated by their high spatio-temporal variability (Minkkinen et al., 2020; Rautakoski et al., 2024). Temporally, fluxes are episodic and strongly influenced by seasonal fluctuations in WTL, water content, temperature, and N availability (Butterbach-Bahl et al., 2013; Pärn et al., 2018; Rautakoski et al., 2024). Short-lived peak events, or 'hot moments', often occur during freeze–thaw transitions or following precipitation, contributing disproportionately to annual N_2O budgets (Rautakoski et al., 2024; Wagner-Riddle et al., 2020). The potential effects of increased harvesting intensity on these emission dynamics warrant further investigation. To date, most studies have relied on infrequent manual sampling during snow-free periods (e.g., Mäkiranta et al., 2012; Maljanen et al., 2003; Peltoniemi et al., 2023; Regina et al., 1998; Tong et al., 2022), while only a few have used automated, year-round measurements (Korkiakoski et al., 2020; Rautakoski et al., 2024). Consequently, this methodological gap has hindered our ability to constrain temporal patterns, controlling factors, and annual budgets of soil N_2O fluxes in boreal drained peatland forests.

Spatially, soil N_2O fluxes are influenced by small-scale heterogeneity in soil properties regulating N cycling (Butterbach-Bahl et al., 2013). Higher emissions in peat soils are commonly associated with deep WTL, low pH, and increased N and phosphorus content and bulk density (Butterbach-Bahl et al., 2013; Liimatainen et al., 2018; Minkkinen et al., 2020; Regina et al., 1996). However, complex interactions among these factors make it difficult to predict soil emissions in forestry-drained boreal peatlands. N_2O production, consumption, and transport also vary with depth (Peltoniemi et al., 2023). These vertical processes are highly complex (Wen et al., 2016) and sensitive to soil properties described above. Given the spatial variability in N availability and fluctuating WTL conditions after harvesting (Korkiakoski et al., 2020, Korkiakoski et al., 2019), further research is needed to clarify controls on net soil surface N_2O emissions across soil depths. Moreover, spatial heterogeneity in soil properties can create localized high-emission zones or 'hot spots' (Wagner-Riddle et al., 2020), potentially biasing ecosystem-scale estimates if not adequately captured. Importantly, inherent spatial variability can be pronounced prior to harvesting and may outweigh immediate harvest effects, as hot spots can develop independently of management actions (Oktarita et al., 2017). Despite its relevance, this remains poorly understood, highlighting a critical knowledge gap for improving N_2O flux assessments in harvested boreal drained peatland forests.

To address current uncertainties, this study evaluates the short-term effects of traditional CC and alternative CCF on soil N_2O fluxes in a nutrient-rich, forestry-drained boreal peatland in southern Finland. Both harvesting sites were implemented in March 2021 and compared against a non-harvested control (C) site. Fluxes were measured using manual chambers during the 2020 (pre-harvest) and 2022 (first post-harvest) growing seasons, and continuously monitored with automated chambers from mid-2020 to late 2022. Complementary measurements of peat physical, chemical, and environmental variables were conducted to support interpretation of flux patterns. Our specific objectives were: 1) to evaluate the short-term effects of CC and CCF on fluxes to identify management implications for climate-smart forestry, and 2) to characterize the temporal and spatial variability of these fluxes and their controlling factors. We hypothesized that: i) fluxes would increase following harvesting, with CC resulting in higher emissions than CCF due to more intense soil disturbance and altered environmental conditions, ii) fluxes would exhibit strong temporal variability, with CC leading to more frequent and intense episodic 'hot moments' than CCF, and iii) spatial heterogeneity would be pronounced, with increased emissions associated with soil properties and environmental conditions. Moreover, inherent spatial variability may exceed harvesting impacts in influencing emission patterns.

2. Materials and methods

2.1. Experimental site

The study was conducted at the Ränskälänkorpi experimental site, a

boreal peatland forest located in the municipality of Asikkala, southern Finland (61°11′N, 25°16′E, 144 m a.s.l.; Fig. 1). Established in 2019, the site functions as a long-term monitoring site for evaluating the effects of contrasting forest harvesting methods on GHG emissions and stand development in forestry-drained boreal peatlands. The local climate is classified as subarctic (Dfc) according to the Köppen–Geiger system. Based on 10 km × 10 km gridded data from the Finnish Meteorological Institute (FMI), the 30-year (1981–2022) mean annual temperature is 4.2 °C, with February being the coldest month (–6.9 °C) and July the warmest (16.5 °C). Mean annual precipitation is 611 mm, and snow cover typically persists 133 days, from early November to late April.

In 2020, the basal area weighted mean stand age at Ränskälänkorpi was 89 ± 6 years (here and hereafter, '±' denotes one standard deviation), indicating that most trees established in the 1930s, concurrent with the initial ditch excavation and gradual drainage of the pristine mire. A secondary ditching phase occurred in the 1960s (exact year unknown), creating open ditches ~1 m deep and spaced ~50 m apart. Since then, no ditch maintenance has been performed, allowing vegetation to partially overgrow most ditches. Additionally, erosion has deepened some ditches over time, including the main channel that flows through the site. Further details on stand age estimation are provided in Supplementary Methods, Section 1.

According to Laine et al. (2012), Ränskälänkorpi is predominantly represented by Herb-rich (Rhtkg II) and *Vaccinium myrtillus* (Mtkg II) drained peatland site types. The peat soil is primarily composed of decomposed sedges (*Carex* spp.) and woody plant material, with an average depth of 1.3 ± 0.7 m (range: 0.4–2.9 m). Mean values (0–50 cm depth) for soil C, N, CN ratio, and bulk density were 52.3 ± 2.3 %, 1.61 ± 0.28 %, 33.7 ± 7.4, and 0.143 ± 0.026 g cm^{-3}, respectively (Supplementary Table S1), indicating a minerotrophic, N-rich peat. Between March and October 2020, the WTL, measured manually relative to the peat surface, ranged from −13 to −103 cm, with a median of −56 [26] cm (here and hereafter, '[]' denotes the interquartile range (IQR)).

Prior to harvesting, the dominant tree species was Norway spruce (*Picea abies* (L.) Karst.), with Scots pine (*Pinus sylvestris* L.) and Downy birch (*Betula pubescens* Ehrh.) present sporadically, either as single trees or in small groups. The tree canopy cover was notably dense, resulting in patchy and variable forest-floor vegetation due to non-uniform light attenuation patterns. Forest-floor vegetation was dominated by ericaceous dwarf shrubs (*Vaccinium myrtillus* L. and *Vaccinium vitis-idaea* L.), herbaceous plants (*Trientalis europaea* L., *Oxalis acetosella* L., *Deschampsia flexuosa* L. Trin., and *Dryopteris carthusiana* (Vill.) H.P. Fuchs), sedges (*Carex globularis* L. and *Eriophorum vaginatum* L.), and a ground layer of mosses (*Hylocomium splendens* (Hedw.) Br. Eur., *Pleurozium schreberi* (Brid.) Mitt., and *Dicranum polysetum* Sw.).

In March 2021, Ränskälänkorpi was divided into three distinct treatment sites (Fig. 1): a non-harvested control site (C, 7.6 ha), a continuous-cover forestry site (CCF, 8.8 ha), and a clear-cutting site (CC, 6.3 ha). Harvesting at the CCF and CC sites was conducted using a harvester and forwarder between 18th March and 1st April 2021, when the peat soil was still frozen. To avoid damaging measurement infrastructure, trees near monitoring equipment at the CCF site were harvested manually (Fig. 1). Additional harvesting in the north-western section of the CC site was completed in June 2021.

Prior to harvesting, stand density (Td) was lower at the CCF and CC sites (1311 and 1008 trees ha^{-1}, respectively) than at the C site (1753 trees ha^{-1}; Fig. 2). However, all sites had comparable stand basal area (BA) values (i.e., 28, 34 and 31 m^2 ha^{-1} for the C, CCF, and CC sites, respectively). At the CC site, nearly all trees were felled. In contrast, the CCF site underwent selection harvesting, resulting in average reductions of 42 % in Td and 57 % in BA. After harvesting, Norway spruce

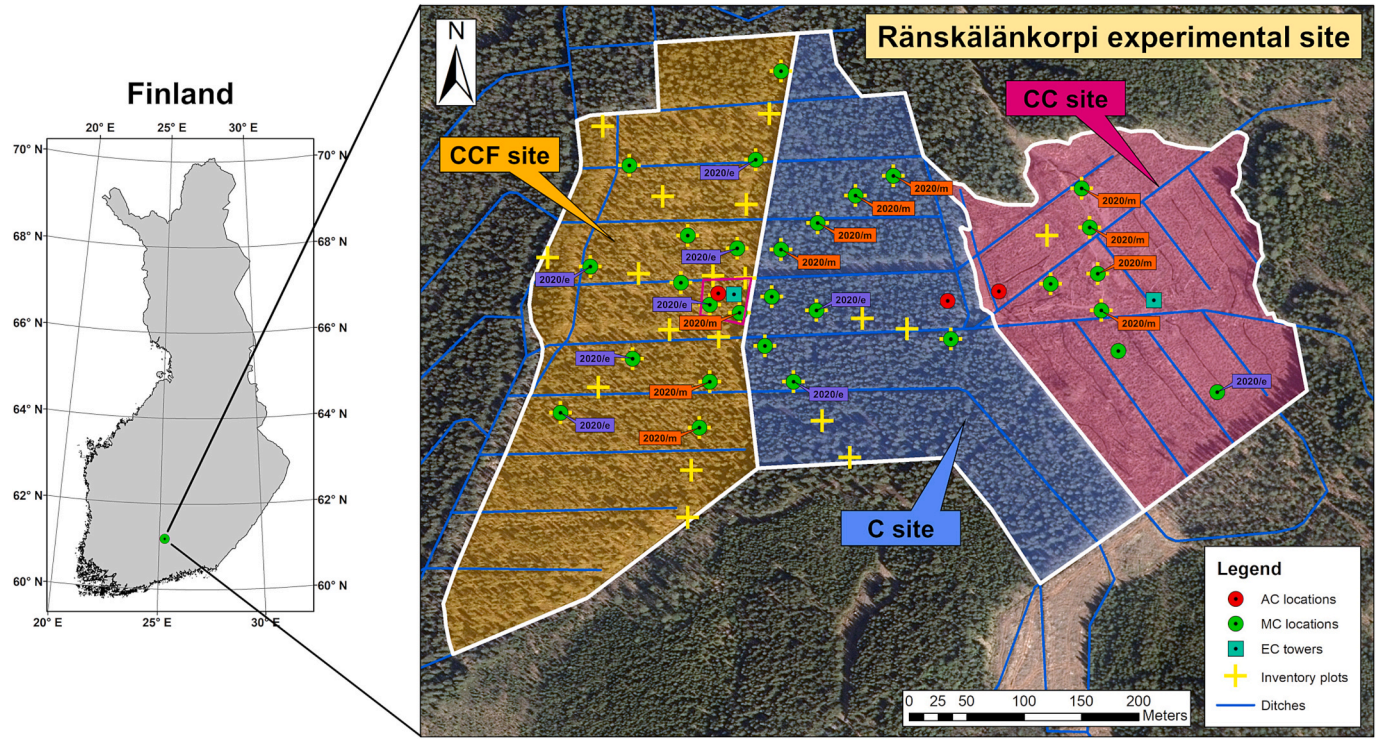

Fig. 1. Overview of the Ränskälänkorpi experimental site. The map of Finland shows the geographical location of the Ränskälänkorpi site. The detailed map illustrates the subdivision of the site into three treatment sites based on harvesting methods: continuous-cover forestry by selection harvesting (CCF), non-harvested control (C), and clear-cutting (CC). Sampling locations for automated chambers (AC, $n = 3$ per site, installed in groups within a 10 m radius), manual chambers (MC, $n = 9$, 7, and 13 at the C, CC, and CCF sites, respectively), eddy-covariance towers (EC, $n = 1$ shared between the C and CCF sites, and $n = 1$ for the CC site), permanent forest inventory plots ($n = 26$, 13, and 6 at the C, CC, and CCF sites, respectively), and drainage ditches are also indicated. MC sampling points in 2020 (pre-harvest) are categorized as either 'measured' ('2020/m', $n = 11$) or 'estimated' ('2020/e', $n = 9$). The magenta outline within the CCF site indicates the manually harvested area implemented in 2021.

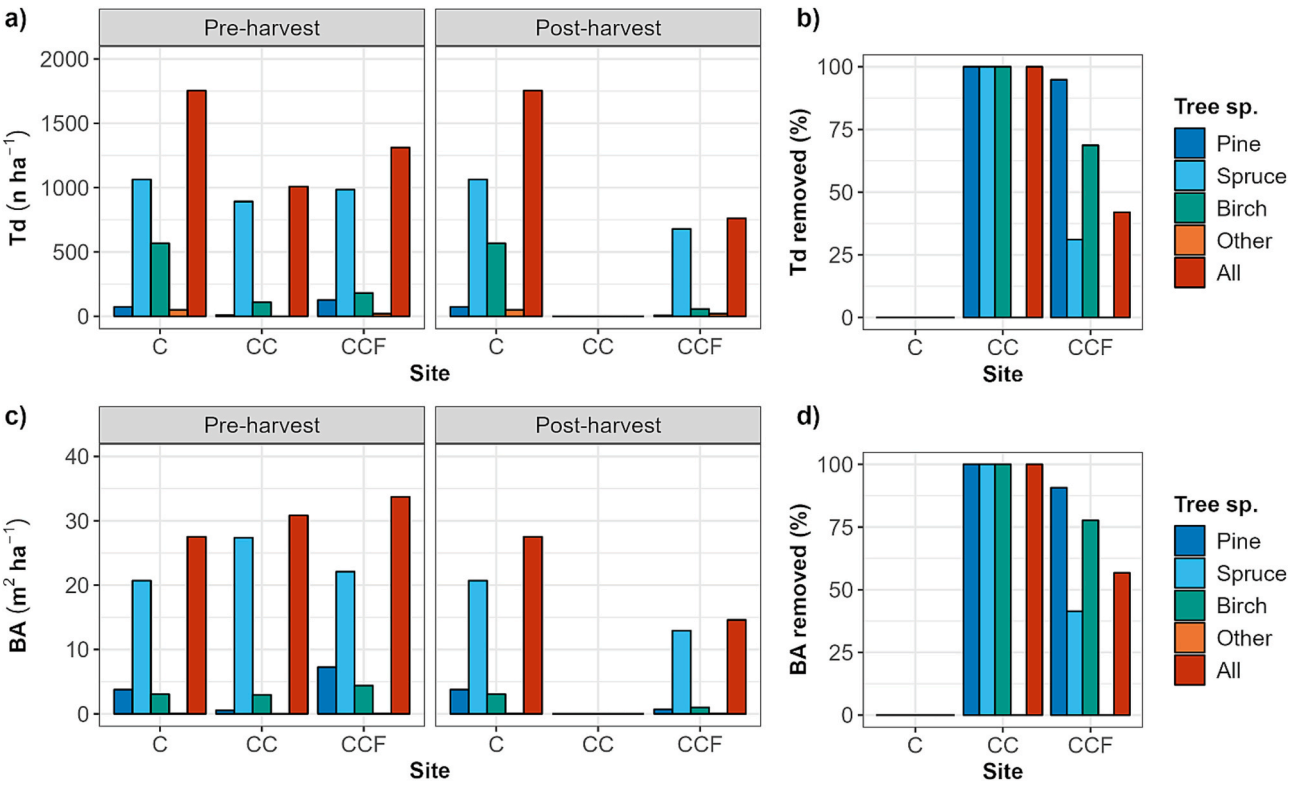

Fig. 2. Pre- and post-harvest forest stand characteristics. Panels show a) stand density (Td), b) percentage of stand density removed, c) stand basal area (BA), and d) percentage of stand basal area removed at C, CC, and CCF sites. Values are shown for individual tree species, including Scots pine ('Pine'), Norway spruce ('Spruce'), Downy birch ('Birch'), and other tree species ('Other'), as well as for the total of all tree species ('All').

accounted for 61 % and 89 % of total Td, and 75 % and 89 % of total BA, at the C and CCF sites, respectively. Some large, dead trees were retained at the CC site, and logging residues (comprising foliage, branches, and stumps) were left on the ground at both the CCF and CC sites. The impact of the harvesting operations on forest-floor vegetation was more pronounced in the CC site than in the CCF site. All original permanent ditches remained intact and were not cleaned, except for small sections crossed by machinery. In summer 2022, the CC site was regenerated using site preparation via ditch mounding, which involved excavating short ($\leq$ 125 m), shallow ditches (20–30 cm deep) to drain surface water away from the regeneration area. Norway spruce seedlings were then planted at a density of approximately 1800–2000 seedlings ha^{-1}.

2.2. Automated chamber-based N_2O flux measurements

2.2.1. Experimental design

Soil-atmosphere N_2O fluxes were measured hourly at each site using a group of three custom-made automated chambers (Fig. 1). At the C and CC sites, the chambers were connected to a shared, climate-controlled instrument cabin, while the CCF site had its own dedicated cabin. At each site, chambers were placed adjacently within a 10 m radius to capture the spatial variability in dominant forest-floor vegetation composition. The timing of automated chamber (AC) based N_2O measurements differed by site (Supplementary Fig. S1). Measurements started at the C site in June 2020 and at the CCF site in October 2020, approximately six months before harvesting. At the CC site, measurements were delayed until September 2021, after the harvesting had already been completed. This study reports AC-based N_2O fluxes up to December 2022.

2.2.2. Technical specifications

The AC system, including chamber structures, tubing, gas analysers, and an instrument cabin, has been previously described and applied in boreal peatland studies (Korkiakoski et al., 2020, 2017; Koskinen et al., 2014; Rautakoski et al., 2024). A full technical description is provided in Koskinen et al. (2014).

In summary, each chamber structure consisted of two rectangular stainless-steel frames, a collar, and a moving chamber. The collar was inserted 2 cm into the peat. During winter, the chamber was elevated above the snowpack using a 16 cm high extension collar. The chamber was a transparent polycarbonate box (57 × 57 × 40 cm; length × width × height) mounted on the upper frame and operated by a linear actuator (model LA35, Linak, Nordborg, Denmark). A 24 V, 8 × 8 cm fan (Maglev KDE2408PTV1, Sunon Ltd., Kaohsiung, Taiwan) was installed on the upper rear side of the chamber, approximately 30 cm above the peat surface, to facilitate air mixing within the chamber headspace. Between measurement periods, the chamber remained upright in close-to-vertical position for ventilation. During snow-covered periods, snow and ice accumulation on chambers and frames were manually cleared every 1–3 weeks, and snow depth within the collars was monitored to adjust chamber volume.

At the C and CC sites, N_2O concentrations were measured using a continuous-wave quantum cascade laser absorption spectrometer (model N2O/CO-23d, Los Gatos Research Inc., Mountain View, CA, USA; precision: 0.1 ppb at 1 s). At the CCF site, a cavity ring-down spectroscopy gas analyser (model G2308, Picarro Inc., Santa Clara, CA, USA; precision: 25 ppb at 1 s) was used. Each chamber was connected to its analyser, situated inside an instrument cabin, in a closed-loop system. The sample air circulated through fluoropolymer inlet (4 mm i.d.) and polyamide outlet (4 mm i.d.) tubing at a flow rate of 1 l min^{-1} using an external pump (either MD 1, Vacuubrand GmbH & Co. KG, Wertheim, Germany, or NMP 830 KNDC, KNF Micro AG, Reiden, Switzerland). Each chamber was closed for 6 min once per hour throughout the year. Between chamber closures, ambient air was measured for 1 min, with additional measurements taken every 30 min to allow gas concentrations in the tubing to equilibrate with ambient levels.

2.2.3. N_2O flux calculation, quality control, and gap-filling

Hourly N_2O fluxes (μg N_2O m^{-2} h^{-1}) were estimated using a linear fit to the change in N_2O concentration during the chamber closure, following the method outlined by Korkiakoski et al. (2017) and detailed in Supplementary Methods, Section 2. Quality control procedures (Supplementary Methods, Section 3) involved removing low-quality data related to system or chamber malfunctions, using a combination of normalised root mean square error (NRMSE) and iterative standard deviation filtering as fit diagnostics.

The AC system occasionally introduced an artificial diurnal N_2O cycle, linked to non-steady-state conditions during periods of low atmospheric turbulence throughout the year. This effect has been previously reported in other peatland forest studies using similar systems (Koskinen et al., 2014; Rautakoski et al., 2024). Thus, daily mean N_2O fluxes were considered the most accurate representation of temporal variation. Subsequently, a quality control procedure was applied to the mean daily fluxes; details are provided in Supplementary Methods, Section 3. To ensure that the hourly data adequately represented sub-daily variations, days with less than 5 hourly measurements were excluded from the calculation of mean daily fluxes for each chamber. Additionally, a Median Absolute Deviation (MAD) test was used to identify and remove potential outliers in the mean daily fluxes, which were primarily caused by sporadic hourly flux peaks.

Following the procedures outlined by Rautakoski et al. (2024), a machine learning approach using a random forest model with conditional inference trees was used to fill data gaps and generate continuous mean daily flux time series for each chamber. Further details can be found in Supplementary Methods, Section 4. Cumulative daily fluxes per chamber were calculated by multiplying daily means by 24 h. Annual cumulative sums for 2021 and 2022 were then obtained by summing the respective daily fluxes.

2.2.4. Ancillary environmental measurements

Below-canopy air temperature (Ta, °C) was measured at 30 cm above the peat surface at each chamber using a radiation-shielded temperature sensor (model PT4T, Nokeval Oy, Nokia, Finland). Peat soil temperature at 5 cm depth (Ts, °C) was simultaneously recorded within each chamber collar using an identical sensor model. Below-canopy photosynthetically active radiation (PAR, μmol m^{-2} s^{-1}) was measured at each chamber with a quantum sensor (model PQS1 PAR Quantum Sensor, Kipp & Zonen, Delft, The Netherlands). Soil moisture at 5 cm depth (Sm, m^3 m^{-3}) was measured at a single location within each group of ACs at each site using a soil moisture sensor (model ML3, Delta-T Devices Ltd., Cambridge, UK).

In the immediate vicinity of the automated chambers at the C and CC sites, WTL was monitored using a hand-held water level meter (Pokela Engineering Services, Helsinki, Finland) from a dip-well (perforated polypropylene tube; 120 cm long, 2 cm diameter) drilled into the peat close to the chamber groups. At the CCF site, WTL was monitored from two separate dip-wells. Manual WTL measurements were conducted on several occasions during 2021 and 2022. Hourly WTL data for each chamber group were subsequently estimated by correlating manual measurements with continuous records from automated loggers installed at multiple locations across the C, CC and CCF sites (see subsection 2.4.).

2.3. Manual chamber-based N_2O flux measurements

2.3.1. Experimental design and N_2O flux calculation

Pre-harvest manual chamber (MC) based N_2O measurements were conducted at the centers of permanent forest inventory plots (8 m radius), defined as 'sampling locations', with 4, 4, and 3 plots at the C, CC, and CCF sites, respectively (Fig. 1). Flux measurements at each sampling location were carried out over 5 campaigns between 10 June and 10 August 2020 (pre-harvest year; see Supplementary Fig. S1). To better characterize soil N_2O fluxes during the first post-harvest year (2022), the number of sampling locations and campaigns were extended. In 2022, MC-based measurements were conducted at the centers of 9, 7, and 13 sampling locations located at the C, CC, and CCF sites, respectively, across 12 campaigns between 3 May and 20 October (Fig. 1 and Supplementary Fig. S1). The number of sampling locations was roughly proportional to site area (7.6, 6.3, and 8.8 ha), ensuring balanced spatial coverage. Plot selection accounted for key gradients influencing N_2O fluxes, including distance from drainage ditches, canopy variability, and stand structure, while avoiding edge effects and spatial clustering. Each sampling location included a single measurement point, selected to represent vegetation cover and species composition at that location.

Fluxes were determined using a custom-made closed opaque cylindrical chamber (30.5 cm height, 32 cm diameter) equipped with a small mixing fan and connected via Teflon tubing in a closed loop to a portable infrared gas analyser (2020: model DX4015, Gasmet Technologies Oy, Vantaa, Finland; precision: 7 ppb at 60 s; 2022: model LI-7820, LI-COR Inc., Lincoln, NE, USA; precision: 0.4 ppb at 1 s). At each measurement point, the chamber was manually placed on the ground, aligned with a pre-cut 2 cm deep ridge along its circumference to ensure an airtight seal. All sampling locations were measured between 10:00 h and 16:00 h during each campaign in 2020 and 2022. Sampling locations were measured in random order during each campaign to prevent diurnal effects.

N_2O concentration was recorded at 1-second intervals over a 3-minute chamber closure period. MC-based N_2O fluxes (μg N_2O m^{-2} h^{-1}) were calculated using a linear fit to the change in N_2O concentration during the chamber closure, analogous to the method applied for ACs (see Supplementary Methods, Section 2). To optimize slope estimation, the first 30 s and last 15 s of each measurement were excluded. Hourly fluxes were assumed representative of mean daily N_2O fluxes.

During each flux measurement, Ts was measured using a hand-held digital thermometer (model ETI Therma 1, Electronic Temperature Instruments Ltd., Worthing, UK). WTL was recorded using the same hand-held water level meter described previously, from a dip-well drilled into the peat.

Because the number of sampling locations was lower in 2020 than in 2022, MC-based N_2O fluxes for 2020 were estimated for 2, 1, and 6 additional sampling locations at the C, CC, and CCF sites, respectively. This approach was based on linear regression analyses conducted among the sampling locations measured within each site in 2022 (see Supplementary Methods, Section 5). Consequently, fluxes in 2020 were measured or estimated at 6, 5 and 9 sampling locations at the C, CC, and CCF sites, respectively. For direct comparison of pre- and post-harvest fluxes, MC measurement campaigns from June-August 2022 (n = 6) were selected across these 20 sampling locations.

2.3.2. Annual cumulative sum

The occurrence of N_2O fluxes is often episodic, and the underlying regulatory processes are inherently complex (Rautakoski et al., 2024). Consequently, deriving accurate estimates of annual cumulative N_2O values from low-frequency MC-based N_2O fluxes and their relationship with environmental variables (e.g., Ts and Sm) presents a significant challenge. To address this, we examined the correlation between the 12 MC-based measurements at each sampling location conducted between May-October 2022 and concurrent AC-based measurements from each automated chamber within each site. This relationship was used to model cumulative N_2O emissions at each MC sampling point separately for the growing season (May–October) and non-growing season (November–April), defining the growing season as the period between the MC campaigns. The annual cumulative sum for 2022 was then calculated for each sampling point by aggregating values across both seasons. Further methodological details are provided in Supplementary Methods, Section 6.

2.4. Other ancillary environmental measurements

Precipitation (P, mm) was monitored at 30-minute intervals at the C site using a weighing rain gauge (model Pluvio^2, OTT HydroMet GmbH, Kempten, Germany) equipped with a wind protection shield. Daily snow depth (S_d, cm) was estimated by the FMI at a nearby weather station (Hämeenlinna Lammi Pappila station, located 18 km southwest of the Ränskälänkorpi experimental site, 61°03′N, 25°02′E, 136 m a.s.l.). These data were used to define the snow-free and snow-covered periods during the study. Subsequently, site-specific daily S_d values were calculated based on punctual S_d measurements taken near the ACs on multiple occasions during the winters from 2021 to 2024. Hourly WTL was monitored using automated pressure transducers (model Odyssey, Dataflow Systems Ltd., Christchurch, New Zealand) installed in perforated plastic tubes at the C ($n = 2$), CC ($n = 2$), and CCF ($n = 1$) sites.

2.5. Soil peat sampling

2.5.1. Topsoil peat sampling

Peat topsoil sampling was conducted in November 2020, with two samples collected from each of the 27 permanent forest inventory plots where MC measurements were performed. Supplementary samples were collected in May 2023 from two additional MC sampling locations at the CC site and from the three AC locations. In both campaigns, sampling points were selected to represent the typical vegetation cover and species composition of each plot and AC group. A volumetric peat profile was collected using a stainless-steel box sampler (100 × 6.3 × 3.9 cm; length × width × height). The sampled layers were 0–10 cm and 10–20 cm below the peat surface. The top 20 cm of peat represents the main production zone for fine roots in boreal peatland forests (He et al., 2023).

All peat samples were dried to constant mass at 105 °C for 48 h. Soil bulk density (BD, g cm^{-3}) was then determined by dividing the oven-dried soil mass by the original sample volume (245.7 cm^{-3}). Total soil C and N concentrations (%) were quantified using a CN analyser (model TruMac CN, LECO Corporation, Saint-Joseph, MI, USA). Concentrations (mg kg^{-1}) of aluminium (Al), boron (B), calcium (Ca), cadmium (Cd), chromium (Cr), copper (Cu), iron (Fe), potassium (K), magnesium (Mg), manganese (Mn), nickel (Ni), phosphorus (P), lead (Pb), sulphur (S), and zinc (Zn) were determined for the 27 sampling locations using a spectrometer (model iCAP 6500 Duo ICP-OES, Thermo Fisher Scientific Ltd., Cambridge, UK) after HNO_3-HCl digestion in a microwave (model Mars 6, CEM Corporation, Matthews, NC, USA). Peat depth (P_d, cm) was also measured in June 2022 at each of the 32 sampling locations by manually inserting a metal rod into the peat until the mineral base was reached.

2.5.2. Deep soil peat sampling

In September 2022, volumetric peat profiles were extracted from a depth of 1 m at 4 permanent forest inventory plots within the C, CC, and CCF sites. The locations of the groups of ACs at the C and CC sites were also sampled. Topsoil peat was collected using the box-type sampler described above, while deeper peat layers were sampled with a Russian-type peat corer consisting of a side-filling chambered sampler (50 cm length, 5 cm inner diameter), an extension metallic rod (1.2 m length), and a T-handle. Peat samples were subdivided into 10-cm subsamples for further analysis. Analyses included pH measurements (in distilled water [1:10, w:v]) and determination of total soil C and N concentrations (%).

2.6. Statistics

Each set of N_2O flux data from the manual and automated chambers was tested for normality using the Shapiro–Wilk test. As neither dataset followed a normal distribution, non-parametric Kruskal–Wallis rank sum tests were applied, followed by Dunn-Bonferroni post hoc tests ($p < 0.05$) to assess differences in soil N_2O fluxes. For repeated chamber measurements, linear mixed-effects models (LMMs) were fitted to asinh-transformed N_2O flux data using restricted maximum likelihood (REML), with day included as a random effect. Pairwise comparisons of estimated marginal means (EMMs) with Bonferroni adjustment ($p < 0.05$) were used to assess differences among chambers. The specific statistical tests applied are indicated in the figure captions. In all figures, boxplots represent the IQR (25th–75th percentiles), with the horizontal line indicating the median and a black cross denoting the mean. Whiskers extend to 1.5 times the IQR, and data points beyond this range are shown as individual outliers.

Non-parametric descriptive statistics, including the median and IQR, were reported for soil N_2O fluxes. Environmental variables (Ta, Ts, PAR, Sm, and WTL) also showed non-normal distributions and were analysed using the same non-parametric approach. For variables with normally distributed data, including stand age, peat depth, peat soil concentrations of C and N, CN ratio, bulk density, and the contribution of the snow-covered period to the annual N_2O balances, the mean and one standard deviation were reported as descriptive statistics.

To identify hot moments of soil N_2O emissions, we applied the 1.5 × IQR method, following the approach recommended by Stuchiner et al. (2025). A single threshold was derived from the complete dataset comprising mean daily N_2O fluxes from all nine ACs across the three sites. Mean daily values exceeding the third quartile (Q3) by more than 1.5 × IQR were classified as hot moments.

To compare MC and AC sampling locations in 2022, hourly N_2O fluxes were extracted from each individual AC for each of the 12 campaigns during which MC measurements were conducted. Fluxes were then averaged for each AC location and campaign. Median campaign values from the 38 MC and 3 AC sampling locations were used to identify N_2O hot spots. Sampling locations with median values exceeding Q3 by more than 1.5 × IQR were classified as hot spots.

A procedure similar to that described by Rautakoski et al. (2024) was used to calculate variable importance (VI) metrics from a random forest model with conditional inference trees. These metrics were used to identify the controlling factors of the temporal variation of soil N_2O fluxes based on AC measurements. To facilitate comparisons across ACs and sites, the VI values of each chamber were normalized (i.e., 0 = least important variable, 1 = most important variable). Non-gap-filled mean daily N_2O data were used in this analysis to avoid the additional uncertainty associated with the gap-filling procedure.

Generalized Additive Models (GAMs) were applied to examine the non-linear relationships between AC-based N_2O fluxes and temporal controlling factors (i.e., Ta, Ts, Sm, WTL, and P) across all sites. The controlling factors of the spatial variation in mean daily N_2O fluxes were identified based on the rank order of individual linear regressions, according to their coefficient of determination (R^2).

To accommodate logistical and technical constraints across different sites and measurement campaigns, we used different gas analysers for MC- and AC-based N_2O measurements. Although no formal cross-comparison was conducted, all instruments were regularly calibrated and verified with certified gas standards. Instrument precision differed substantially, and we therefore acknowledge that instrument-specific variability could contribute to minor differences in measured N_2O concentrations, particularly at the C site where fluxes are near zero. Nonetheless, we consider these differences unlikely to substantially affect overall flux estimates or comparisons across sites, ensuring consistency and reliability across datasets.

AC-based N_2O fluxes were calculated using the Python programming language (version 3.9, Van Rossum and Drake, 2009). Data preparation, analysis, and visualization were conducted in R (version 4.3.3, R Core Team) and RStudio (version 2022.07.2, Posit PBC), using the following packages: *Cforest*, *corrplot*, *cowplot*, *dplyr*, *emmeans*, *FSA*, *ggplot2*, *ggpmisc*, *ggpubr*, *mgcv*, *multcompView*, *nlme*, *party*, *PerformanceAnalytics*, *rcompanion*, *reshape2*, and *tidyverse*.

3. Results

3.1. Effects of harvesting methods on forest-floor environmental conditions

At the C site, median annual Ta and Ts remained consistent between 2021 (harvest year) and 2022 (first post-harvest year), averaging 3.6 °C and 2.8 °C, respectively (Fig. 3a–b). At the CCF site, harvesting led to an increase in both Ta and Ts in 2021, followed by a slight decrease in 2022. In contrast, the CC site exhibited a notable rise in Ta, but especially in Ts, in 2022.

Median annual PAR at the C site remained stable across 2021–2022, at approximately 11 μmol m^{-2} s^{-1} (Fig. 3c). After harvesting, PAR increased markedly, by ~2.5-fold at the CCF site (averaging 25 μ mol s^{-1}) and nearly ninefold at the CC site (96 μmol m^{-2} s^{-1}).

In 2021, median annual Sm at the C site was slightly higher than in 2022 (0.28 vs. 0.19 m^3 m^{-3}; Fig. 3d). After harvesting, Sm increased by 0.06 m^3 m^{-3} at the CC site and showed a more pronounced increase at the CCF site, averaging 0.12 m^3 m^{-3}.

Median annual WTL, measured relative to the peat surface, was shallower at the C site in 2021 (–37 cm) than in 2022 (–47 cm; Fig. 3e). At the CC site, WTL was –29 cm in 2021 and –26 cm in 2022, while at the CCF site, values remained relatively stable (–49 and –50 cm, respectively). These results indicate that harvesting generally led to a rise in WTL in both years, with a more pronounced effect at the CC site than at the CCF site. Notably, growing season WTL measurements, which capture larger spatial variability, support this harvesting-induced raise (Supplementary Fig. S2). Specifically, the median growing season WTL increased by 13 cm at the CC site from the pre-harvest year 2020 to the first post-harvest year 2022, whereas the increase at the CCF site was more modest, at 6 cm over the same period.

3.2. Dynamics and controlling factors of the temporal variability of soil N_2O fluxes

Manual chamber-based measurements conducted during June-August in 2020 and 2022 (Fig. 4) revealed increased median soil N_2O fluxes in the first year after harvesting at both the CC and CCF sites compared to the pre-harvest year. Specifically, fluxes rose from 11 [47] to 30 [26] μg N_2O m^{-2} h^{-1} at the CC site, and from 6 [111] to 54 [94] μg

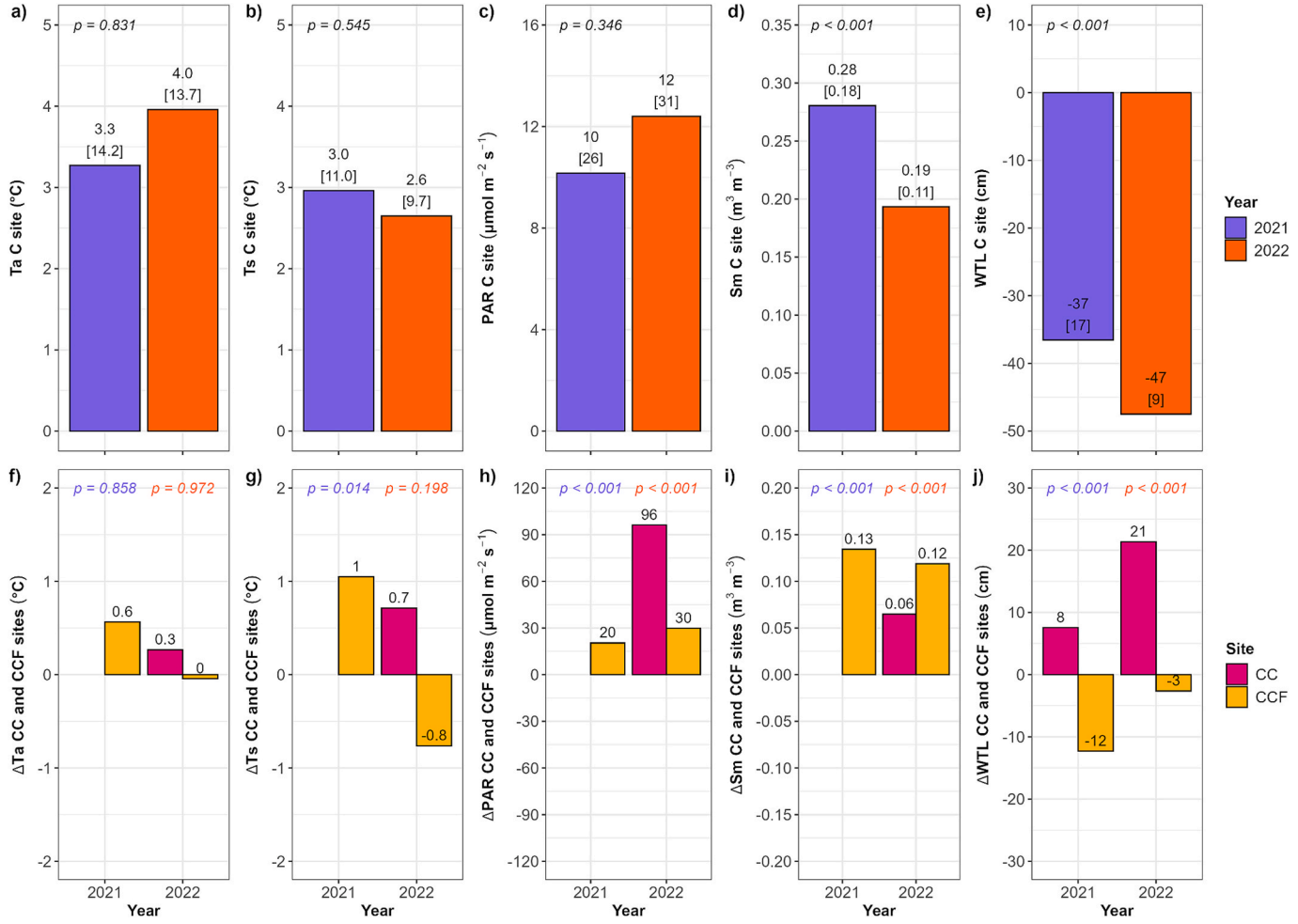

Fig. 3. Effects of harvesting methods on forest-floor environmental conditions. Panels a)–e) show the annual median values (with interquartile ranges in brackets) of below-canopy air temperature (Ta), soil temperature at 5 cm depth (Ts), below-canopy photosynthetic active radiation (PAR), soil moisture at 5 cm depth (Sm), and water table level (WTL) at the C site during the harvest year (2021) and the first post-harvest year (2022). Note that early 2021 represents pre-harvest conditions, with harvesting beginning in March. For consistency, 2021 is considered a post-harvest year since most of the year reflects post-harvest conditions and associated effects. Panels f)–j) show the absolute changes (ΔX) in these variables at the CC and CCF sites, calculated as $\Delta X_{CC} = X_{CC} - X_C$ and $\Delta X_{CCF} = X_{CCF} - X_C$. Positive and negative ΔX values represent increases and decreases relative to the C site, respectively. Note that ΔTa, ΔTs, ΔPAR, ΔSm values for the CC site are presented only for 2022. *p*-values in panels a)–e) indicate differences between years at the C site, based on non-parametric Kruskal–Wallis rank sum tests; *p*-values in panels f)–j) indicate differences between sites within each year, also based on Kruskal–Wallis tests. Ta, Ts, PAR, and Sm data were obtained from measurements inside or near automated chambers, while WTL data also included measurements from other site locations.

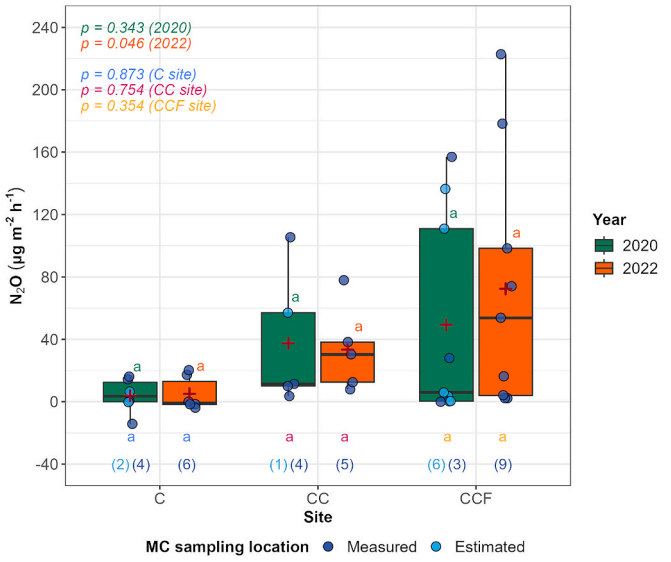

Fig. 4. Pre- and post-harvest soil N_2O fluxes. Mean daily N_2O fluxes are shown for the C, CC, and CCF sites during the pre-harvest year (2020) and the first post-harvest year (2022). Data include MC 'measured' and 'estimated' fluxes collected from June-August 2020, and MC 'measured' from June-August 2022. For each year and site, *p*-values from non-parametric Kruskal–Wallis rank sum tests are shown. Different superscript letters denote significant differences between sites (within boxes) or between years (below boxes), based on Dunn-Bonferroni post hoc tests ($p < 0.05$). Values in parentheses indicate the total number of 'measured' and 'estimated' sampling locations per site and year.

N_2O m^{-2} h^{-1} at the CCF site, although these increases were not statistically significant. In contrast, the C site exhibited minimal change, with median flux values shifting from 4 [12] to –1 [15] µg N_2O m^{-2} h^{-1}.

Automated chamber-based measurements revealed that daily mean N_2O fluxes at the C site remained near neutral throughout the study period (June 2020 to December 2022), ranging from –18 to 26 µg N_2O m^{-2} h^{-1} (min–max values, Fig. 5a,d), and no hot moments were detected (Fig. 5a). In contrast, the CC site exhibited substantial temporal variability between September 2021 and December 2022, with daily mean fluxes ranging from –12 to 278 µg N_2O m^{-2} h^{-1} (Fig. 5b,e), and hot moments occurring on 14.9 ± 5.7 % of measured days (Fig. 5b). At the CCF site, daily mean N_2O fluxes ranged from –24 to 109 µg N_2O m^{-2} h^{-1} between October 2020 and December 2022 (Fig. 5c,f), with hot moments accounting for 11.7 ± 5.9 % of measured days (Fig. 5c). The contribution of hot moments to the annual cumulative N_2O balance at the CCF site was substantially lower in the harvest year 2021 than in the first post-harvest year 2022, increasing from 25 ± 4 % to 61 ± 16 % (Fig. 5i). In 2022, hot moments contributed more to the annual balance at the CC site (71 ± 20 %) than at the CCF site (61 ± 16 %; Figs. 5h,i).

The key factors controlling the temporal variability of AC-based N_2O fluxes differed markedly between non-harvested and harvested sites (Fig. 6a). Specifically, at the C site, Ta and P were dominant, with mean VI values of 0.70 and 0.64, respectively (0 = no importance, 1 = high importance). In contrast, WTL was a key driver at the CC and CCF sites (VI = 0.46 and 0.53, respectively), while Sm was the most influential factor at the CCF site (VI = 0.59). Lagged and cumulative effects of different controlling factors were also associated with the temporal variability of fluxes, particularly at the harvested sites (Fig. 6b). At the CCF site, lagged WTL, Sm, and Ts had substantial influence, with VI values of 0.46, 0.45, and 0.41, respectively, corresponding to peak predicted fluxes at lags of 3, 1 and 4 days, respectively (Supplementary Fig. S3). Similarly, at the CC site, lagged WTL and Sm (VI = 0.46 and 0.44, respectively) were most influential at lags of 7 and 1 days, respectively. Cumulative precipitation was also associated with peak fluxes at 4 and 7 days at the CC and CCF sites, respectively.

Generalized additive model (GAM) effect splines were used to explore the relationship between AC-based N_2O fluxes and temporal controlling factors (Supplementary Fig. S4). At the C site, the consistently low flux magnitudes limited the ability to identify significant relationships. At the CC site, peak fluxes corresponded to optimal Ta and Ts values of about 19 and 16 °C, respectively. At the CCF site, relationships with Ta and Ts were more complex, exhibiting two distinct peaks: one at low temperatures (Ta ~–4 °C, Ts ~–1 °C), and another at higher temperatures (Ta ~16 °C, Ts ~15 °C). Sm also played an important role, with increased fluxes observed when Sm ranged between 0.25 and 0.27 at the CC site and 0.24–0.28 m^3 m^{-3} at the CCF site. Additionally, fluxes at the CC site peaked when WTL was around –33 cm. At the CCF site, the N_2O-WTL relationship was more variable, exhibiting three distinct flux peaks at WTL depths of –12, –42, and –56 cm.

3.3. *Dynamics and controlling factors of the spatial variability of soil N_2O fluxes*

Manual chamber-based measurements carried out during June-August in 2020 and 2022 revealed varying degrees of spatial variability in soil N_2O fluxes across the three study sites (Fig. 4). Specifically, spatial heterogeneity increased in the order: C → CC → CCF. This spatial pattern remained consistent across both pre- and post-harvest years at each study site.

This pronounced spatial variability was further investigated using combined data from 38 sampling locations (9 ACs and 29 MCs) collected in 2022 (Fig. 7). The range of N_2O fluxes (min–max) was –38 to 54, –5 to 261, and –39 to 459 µg N_2O m^{-2} h^{-1} at the C, CC, and CCF sites, respectively. The C site exhibited the highest spatial homogeneity and the most frequent occurrence of low-flux locations. Median fluxes across the C site locations ranged from –5 [4] to 14 [16] µg N_2O m^{-2} h^{-1}. In contrast, the CC site showed greater spatial heterogeneity, including several locations with high fluxes and two identified as hot spots, with median values ranging from 2 [8] to 88 [72] µg N_2O m^{-2} h^{-1}. The CCF site exhibited the greatest spatial variability, with median fluxes ranging from 0 [5] to 149 [208] µg N_2O m^{-2} h^{-1} and the highest number of hot spots ($n = 3$), two of which showed the highest fluxes observed across all study sites.

Correlation analysis identified several factors controlling the spatial variability of N_2O fluxes (Fig. 8). Positive correlations were observed with K ($R^2 = 0.32$, r = 0.57), Cu ($R^2 = 0.17$, r = 0.41), P ($R^2 = 0.15$, r = 0.39), and BD ($R^2 = 0.11$, r = 0.33). Marginal positive correlations were also found with Ts ($R^2 = 0.10$, r = 0.32) and N ($R^2 = 0.09$, r = 0.30), while a marginal negative correlation was observed with the CN ratio ($R^2 = 0.08$, r = –0.29). GAMs indicated linear relationships between N_2O fluxes and most variables, except for K and Cu, which exhibited non-linear trends (Supplementary Fig. S5). Furthermore, the results indicated that correlations between N_2O fluxes and soil variables (K, Cu, P, BD, N, and CN ratio), were stronger in the deeper peat layer (10–20 cm) than in the topsoil layer (0–10 cm). Significant correlations were primarily observed in the deeper layer, while those in the topsoil were generally weaker or non-significant. Apart from Ts, no significant differences were observed among the C, CC, and CCF sites regarding the temporal controlling factors of N_2O fluxes (Supplementary Fig. S6).

Deep peat soil sampling at 10 cm depth intervals enabled assessment of C, N, CN ratio and pH as potential controlling factors (Fig. 9). No clear trends were observed between C or pH and N_2O fluxes across the soil peat profile. In contrast, correlations between N and CN ratio with N_2O fluxes (positive and negative, respectively) were notably stronger in soil peat layers located above the WTL at all the study sites. During the 2022 growing season, WTL depths were –58 [41] cm, –29 [12] cm, and –56 [13] cm at the C, CC, and CCF sites, respectively (Supplementary Fig. S7). Notably, peak values of these correlations were consistently observed just above the WTL.

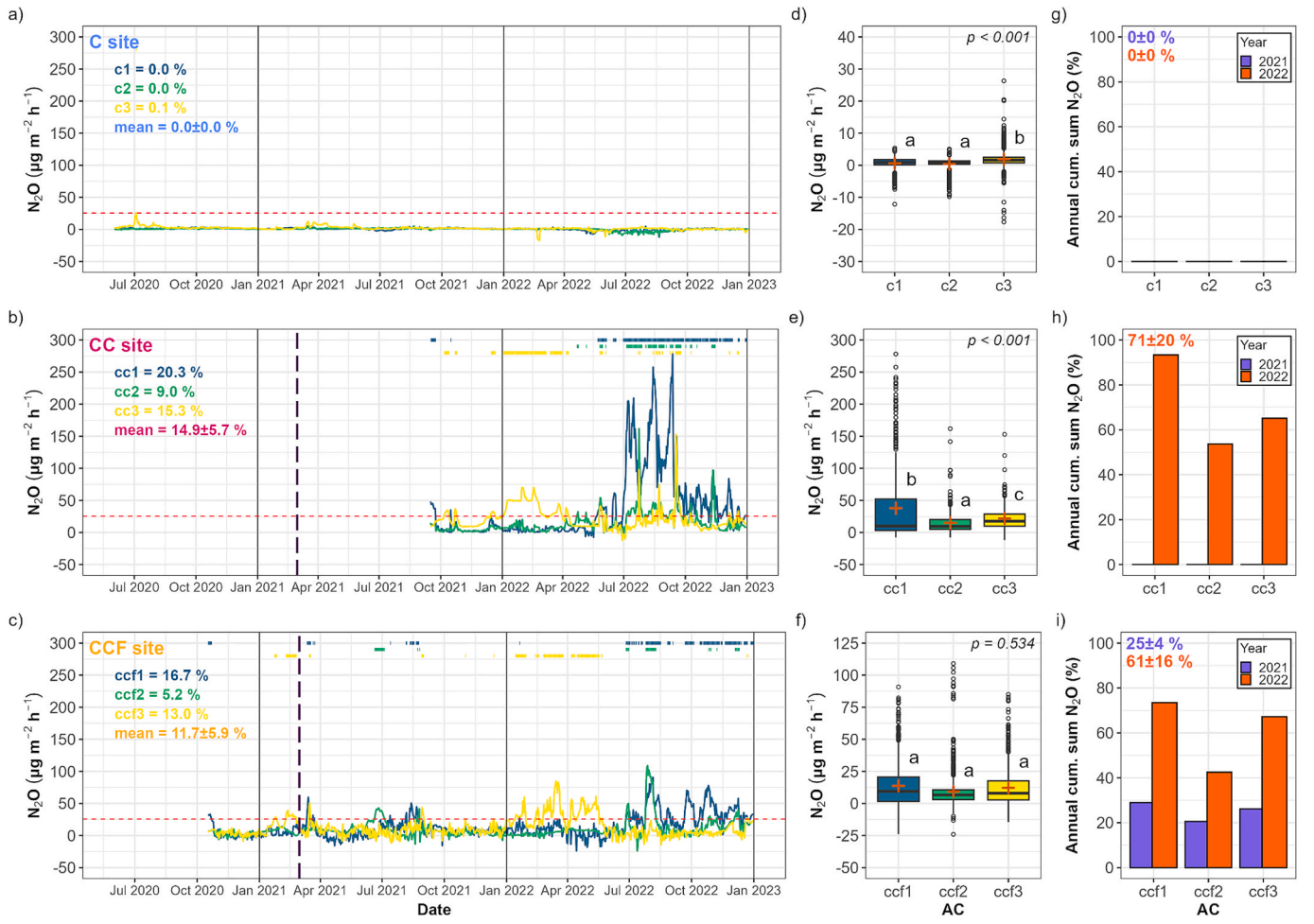

Fig. 5. Temporal variation in soil N_2O fluxes. Panels a), b), and c) show time series of mean daily N_2O fluxes measured by each AC at the C, CC, and CCF sites, respectively. The purple dashed vertical lines in panels b) and c) indicate the timing of the harvesting treatment initiation. The truncated lines at the top of each panel indicate periods identified as hot moments for each AC. The red horizontal line in each panel represents the threshold for defining hot moments (25.6 µg N_2O m^{-2} h^{-1}). Values indicate the proportion of hot moments for each AC and the mean value for each site. Panels d), e), and f) display box-plots of mean daily fluxes measured by each AC at the C, CC, and CCF sites, respectively. For each site, the *p*-value corresponds to the fixed effect of chamber from a linear mixed-effects model (REML) with day as a random effect to account for repeated measures. The model was fitted on asinh-transformed N_2O flux data. Different superscript letters denote significant differences among chambers (EMM pairwise comparisons, Bonferroni-adjusted $p < 0.05$). Panels g), h), and i) present the contribution of hot moments to the annual cumulative N_2O flux for each AC and the mean value for each site in 2021 (harvest year) and 2022 (first post-harvest year).

3.4. Annual cumulative soil N_2O fluxes

Automated chamber-based measurements indicated that the annual N_2O balance at the C site was close to neutral in both the harvest year 2021 and the first post-harvest year 2022, with median values of 11 [6] and –5 [5] mg N_2O m^{-2} y^{-1}, respectively (Fig. 10a–b). The annual balance was higher at the CCF site than at the C site in both years, reaching 72 [7] mg N_2O m^{-2} y^{-1} in 2021 and 145 [43] mg N_2O m^{-2} y^{-1} in 2022. The CC site showed the highest annual balance among the sites in 2022 (157 [150] mg N_2O m^{-2} y^{-1}).

The snow-covered period contributed similarly to the annual balances at the C and CCF sites in 2021 (32 ± 10 % and 39 ± 11 %, respectively; Supplementary Fig. S8). In 2022, the longer snow cover duration and greater snowpack depth enhanced the contribution of the snow-covered period to annual N_2O fluxes, reaching values close to 44–48 %. Although the CC site exhibited a substantially deeper snowpack in 2022 than the C and CCF sites, its relative contribution from the snow-covered period was lower, at 29 ± 26 %.

In addition to AC-based measurements, the annual site-level balances in 2022 were Supplemented with estimates derived from MC-based measurements (Fig. 10c). Considerable spatial variability was observed, with individual location values (min–max) ranging from –11 to 39 mg N_2O m^{-2} y^{-1} at the C site, 44 to 704 mg N_2O m^{-2} y^{-1} at the CC site, and 10 to 1513 mg N_2O m^{-2} y^{-1} at the CCF site. Overall, the annual balance increased with harvest intensity in the order C → CCF → CC, with median values of 0 [25], 163 [533], and 185 [194] mg N_2O m^{-2} y^{-1}, respectively. However, the difference between the CCF and CC sites was not statistically significant. Notably, the large IQR values observed for annual emissions, particularly at the CCF site, exceeding the median, reflect substantial spatial variability primarily driven by localized hot spots with disproportionately high N_2O fluxes.

4. Discussion

4.1. Temporal variability of soil N_2O fluxes

4.1.1. Forestry-drained boreal peatland as a consistent source of N_2O

Soil N_2O fluxes at the Ränskälänkorpi experimental site exhibited notable temporal variability, with daily mean values ranging from − 39 to 459 µg N_2O m^{-2} h^{-1} (Figs. 5 and 6), consistent with previously reported ranges (−7 to 450 µg N_2O m^{-2} h^{-1}) for forestry-drained boreal peatlands across Finland with soil CN ratios of 16.0–45.0 (Ojanen et al., 2010). These findings indicate that the studied peatland predominantly acts as a net N_2O source.

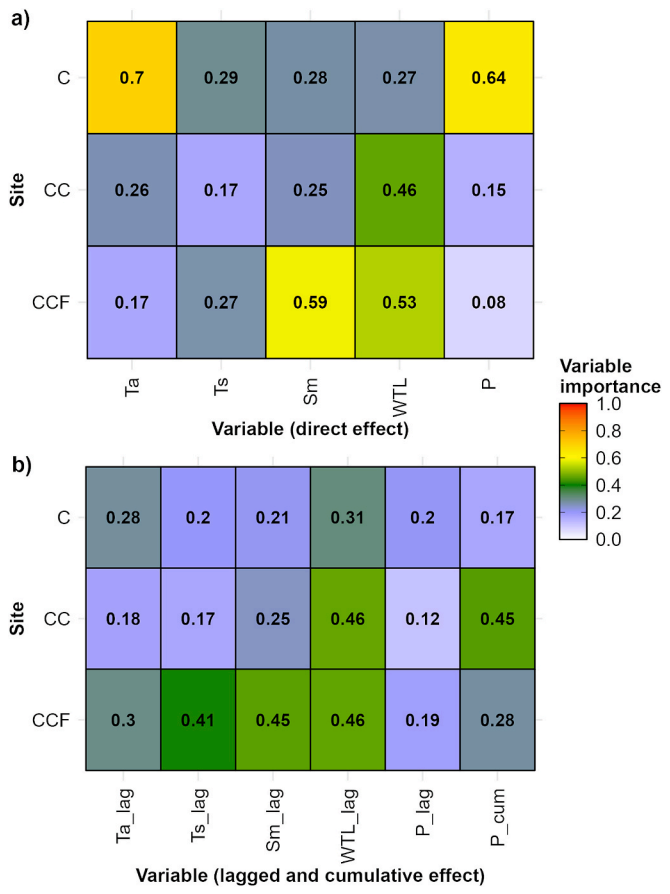

Fig. 6. Controlling factors of the temporal variation in soil N_2O fluxes. Panels show the variable importance (VI) values from random forest models with conditional inference trees, showing the drivers of temporal variation in mean daily N_2O fluxes at the C, CC, and CCF sites. Panel a) presents the direct effects of mean daily below-canopy air temperature (Ta, °C), mean daily soil temperature at 5 cm depth (Ts, °C), mean daily soil moisture at 5 cm depth (Sm, m^3 m^{-3}), mean daily water table level (WTL, cm), and cumulative daily precipitation (P, mm). Panel b) presents the mean lagged effect (1–7 days) of these variables (Ta_lag, Ts_lag, Sm_lag, WTL_lag, and P_lag, respectively), as well as the cumulative effect of cumulative daily P during the previous 1–7 days (P_cum). Values represent the mean VI of the 3 ACs per site. Higher VI values indicate stronger temporal control on fluxes. Note that flux data were derived from non-gapfilled AC measurements. The time periods covered are as follows: C site – entirely under non-harvested conditions; CC site – entirely post-harvest; CCF site – includes both pre-harvest (October 2020–March 2021; 17 ± 3 % of total dataset) and post-harvest (April 2021–December 2022; 83 ± 3 %) periods.

Interestingly, some areas within the C site exhibited small N_2O sink, even on an annual scale. AC-based soil N_2O fluxes fluctuated between weak emissions (max: 26 μg N_2O m^{-2} h^{-1}) and limited uptake (min: –18 μg N_2O m^{-2} h^{-1}), similar to fluxes reported for natural and drained boreal peatlands with varying nutrient status (Pihlatie et al., 2010; Regina et al., 1996). Low emissions at the C site likely reflect limited soil N availability, particularly NO_3^- (Supplementary Fig. S9). Nitrification, which produces both NO_3^- and N_2O, was probably suppressed by NH_4^+ competition with trees and forest-floor vegetation. However, mechanisms driving N_2O uptake, which represented ~16 ± 7 % of daily observations and occurring evenly between May-September, remain uncertain. The high-sensitivity analyser at this site (minimum detectable flux: 0.1 μg N_2O m^{-2} h^{-1}) enabled detection of small fluxes while minimizing instrumental noise issues (Cowan et al., 2014). Reduced N_2O production in the oxic layer may have shifted fluxes from emission to uptake, possibly via dissimilatory N_2O reduction in deeper anoxic peat layers (Chapuis-Lardy et al., 2007). Alternatively, N_2O consumption in the oxic layer could have occurred through N_2O fixation (i.e., assimilation), potentially triggered by N limitation (Si et al., 2023). Beyond these processes, other microbial pathways may also contribute. Dissimilatory nitrate reduction to ammonium (DNRA) can reduce N_2O production by diverting nitrate away from denitrification, particularly under low NO_3^- availability and high C:NO_3^- ratios, as observed at the C site (Pandey et al., 2020). Co-denitrification, which involves the hybrid production of N_2 from both NO_2^- and organic N compounds, may also result in direct N_2 formation without intermediate N_2O release (Wilson et al., 2021). Yet, both DNRA and co-denitrification have been also shown to produce N_2O but their relative contributions to N_2O emissions are unclear (Giles et al., 2012). These uncertainties highlight the need for targeted microbial and isotopic investigations, along with studies on soil redox potentials and vertical N_2O dynamics within the peat profile, to better understand the processes facilitating N_2O uptake.

4.1.2. *Clear-cutting increases frequency and intensity of soil N_2O emissions*

Automated chamber-based fluxes exhibited pronounced seasonal variability, peaking in summer and lowest during the snow-covered period (Fig. 5). The substantial contribution of the snow-covered period to the annual N_2O balance, and its implications for future research, are detailed in Supplementary Discussion, Section 1. During summer, hot moments were more frequent and intense at the CC site than at the CCF site, likely due to clear-cutting effects. First, more decomposing logging residues and reduced N uptake from lower plant biomass at the CC site (Fig. 2) may have increased available N in the soil surface (Mäkiranta et al., 2012). Second, higher Ts at the CC site (Fig. 3g), driven by greater solar exposure after canopy removal (Fig. 3h), likely accelerated peat decomposition, potentially reducing O_2 availability while increasing N mineralization (Maljanen et al., 2003). Third, a greater WTL rise at the CC site (Fig. 3j), resulting from lower transpiration due to reduced plant biomass, may have promoted anoxic conditions favouring N_2O production via denitrification (Regina et al., 1996).

Overall, post-harvest median emissions showed a non-significant increase at both CC and CCF sites relative to pre-harvest conditions (Fig. 4). These emissions may stabilize or decline as the forest ecosystem recovers through gradual changes in nutrient uptake, soil environmental conditions, and/or residue decomposition dynamics (Zhang et al., 2022a). Nonetheless, clear-cutting impacts may persist longer than those of selection harvesting. Further long-term monitoring is needed to draw conclusive insights and evaluate the sustained effects of different harvesting practices on soil N_2O dynamics in forestry-drained boreal peatlands.

4.1.3. *Controlling factors of temporal variability of soil N_2O fluxes*

Our results highlight complex interplay of factors regulating the temporal variability of soil N_2O fluxes. Notably, primary temporal controlling factors were partly different between the C site and the harvested sites (Fig. 6a). At the C site, fluxes correlated more with Ta than Ts, suggesting that active N_2O-producing microbes may reside predominantly in the upper peat layer, consistent with previous studies (Pihlatie et al., 2010; Regina et al., 1998). Pronounced temporal flux responses to soil rewetting after precipitation further supports this interpretation, though caution is warranted given low flux magnitudes. Greater temporal variation in Ta than Ts may have caused our modelling approach to emphasize the Ta–N_2O relationship, partially accounting for its higher apparent importance. In contrast, at the CC and CCF sites, WTL and Sm were key factors, regulating O_2 availability for microbial processes (Butterbach-Bahl et al., 2013), as documented in peat soils (e.g., Peltoniemi et al., 2023; Rautakoski et al., 2024). GAM analysis further indicated that fluctuations around intermediate Ts and Sm, as well as deep WTL, increase N_2O emissions (Supplementary Fig. S4). A detailed discussion of these relationships at the CC and CCF sites is provided in Supplementary Discussion, Section 2. Although 17 ± 2 % of the non-gapfilled AC dataset at the CCF site represents pre-harvest

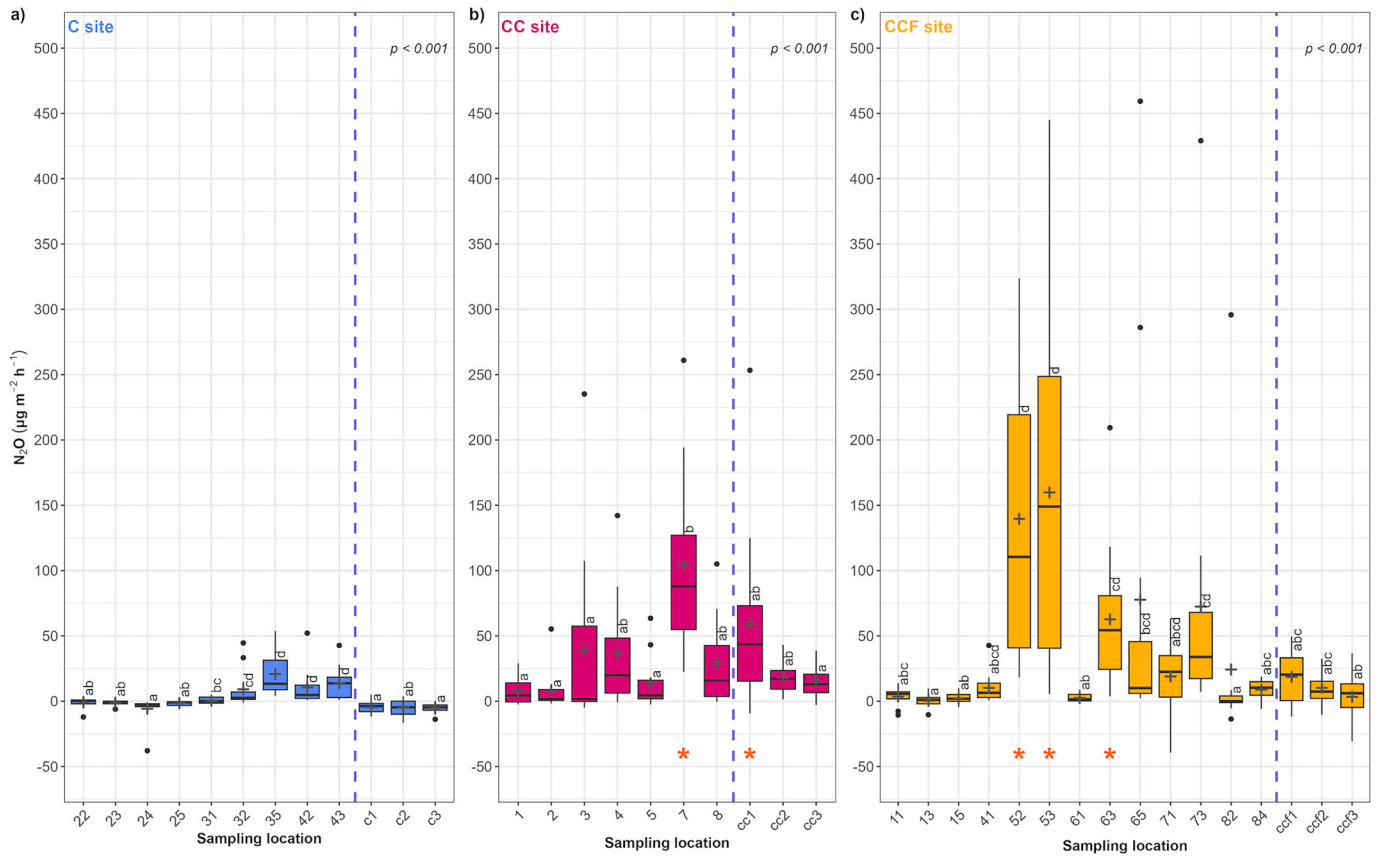

Fig. 7. Spatial variation in soil N_2O fluxes. Panels show the box-plots of mean daily N_2O fluxes at MC and AC sampling locations during the 2022 growing season at a) C, b) CC, and c) CCF sites. For each site, the *p*-value corresponds to the fixed effect of chamber from a linear mixed-effects model (REML) with day as a random effect to account for repeated measures. The model was fitted on asinh-transformed N_2O flux data. Different superscript letters placed vertically above each boxplot denote significant differences among chambers (EMM pairwise comparisons, Bonferroni-adjusted $p < 0.05$). The dashed vertical line in each panel separates MC and AC sampling locations. Asterisks below the boxes identify hot spots. Sample size: $n = 12$ flux measurements in each sampling location from 3 May to 20 October 2022.

conditions, results mainly reflect post-harvest. At the CC site, late AC initiation missed early 2021 post-harvest emissions, so temporal patterns may not capture the full post-harvest trajectory. Despite these limitations, our findings emphasize the critical role of hydrological and thermal conditions in controlling temporal N_2O flux dynamics, underscoring their sensitivity to harvesting and even moderate environmental fluctuations.

4.1.4. Temporal variability of soil N_2O fluxes driven by lagged environmental responses

The influence of environmental controls on the temporal modulation of soil N_2O fluxes may not be immediate. Instead, time-lagged responses to Ts, Sm, WTL, and/or precipitation may also play a crucial role in determining emission timing and magnitude in boreal peat soils (Rautakoski et al., 2024). In this study, soil N_2O emissions typically peaked one day after the peak in Sm measured at 5 cm depth across all sites (Supplementary Fig. S3). This short lag likely reflects the high permeability of the topsoil peat, facilitating rapid water infiltration and O_2 diffusion (Könönen et al., 2015), which promotes anoxic conditions and stimulates microbial processes. In contrast, peak emissions occurred with a longer lag of ~3–4 days following the peak in WTL at the CC and CCF sites (Supplementary Fig. S3). This delay may result from the slower rise of the WTL from deeper peat layers after precipitation, with moisture changes becoming fully effective only after microbial communities have adjusted, causing a postponed emission peak. We also observed a lag of around 4–5 days between Ts and N_2O emissions at the C and CCF sites (Supplementary Fig. S3), suggesting a more indirect role of temperature in regulating N_2O fluxes, compared to the more immediate effects of water availability (Pärn et al., 2018).

Precipitation often triggers N_2O pulses (Rautakoski et al., 2024), but magnitude and pathway (nitrification vs. denitrification) depend on event size and duration (Gao et al., 2024). In our study, emissions were not clearly linked to individual precipitation events at the CC and CCF sites (Fig. 6a) but responded to cumulative precipitation over 4 and 7 days, respectively (Supplementary Fig. S3). The shorter response period at the CC site may result from canopy removal, which likely amplifies fluctuations in Sm and O_2 availability, leading to more rapid microbial responses that are further accelerated by elevated N availability and more pronounced drying-rewetting cycles (Peltoniemi et al., 2023; Sarkkola et al., 2010). These dynamics could have important implications for climate change and the global N cycle, particularly in the Nordic region, where precipitation is projected to become more frequent and intense, especially in summer months (Dyrrdal et al., 2023). Given the higher frequency and intensity of hot moments at the CC site compared to the CCF site, our results suggest that selection harvesting, by maintaining greater canopy cover, may help stabilize Sm and reduce N_2O sensitivity to precipitation, thereby supporting climate mitigation efforts.

4.2. Spatial variability of soil N_2O fluxes

4.2.1. Hot spots as key determinants of large spatial variability in soil N_2O fluxes

Considerable spatial variability in soil N_2O fluxes was observed across sites (Fig. 4). Intra-site spatial variability, measured by the IQR, was on average 3 and 8 times greater at the CC and CCF sites,

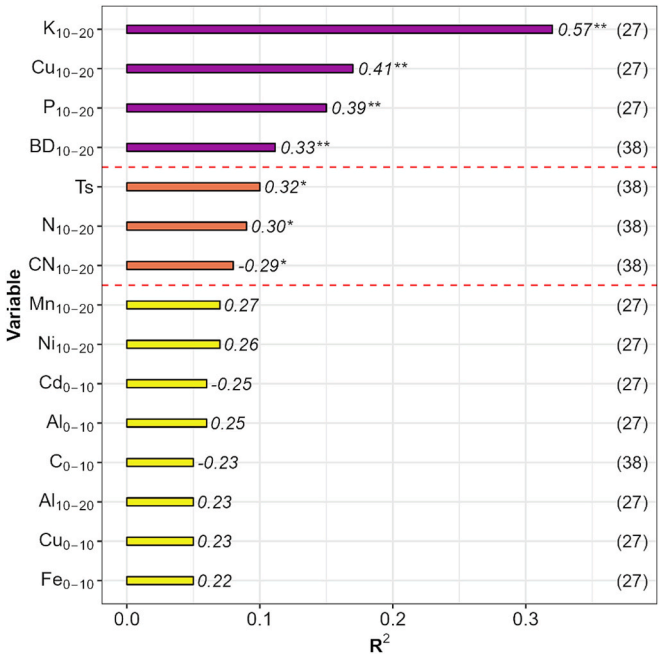

Fig. 8. Controlling factors of the spatial variation in soil N_2O fluxes. Correlation analysis ranking the 15 most influential variables explaining the spatial variation of mean daily N_2O fluxes during the 2022 growing season, combining MC and AC data. Variables include soil concentrations (mg kg^{-1} or %) of K, Cu, P, N, Mn, Ni, Al, Cd, C, and Fe, as well as the CN ratio, soil bulk density (BD, g cm^{-3}), and soil temperature at 5 cm depth (Ts, °C), specified by sampling depth (0–10 cm and 10–20 cm). Variables are ranked by coefficient of determination (R^2) from individual correlations with N_2O fluxes. Italicized values indicate Pearson's correlation coefficients; two asterisks for significance ($p < 0.05$), one for marginal ($p < 0.1$), none for non-significant. Coloured bars and red dashed lines indicate correlation groups. Sample sizes are shown in parentheses ($n = 27$ MC sampling locations, $n = 38$ combined MC + AC sampling locations).

respectively, than at the C site. Combined MC and AC measurements from 2022 indicate that this variation is largely driven by N_2O hot spots (Fig. 7). Although representing only ~20 % of sampling locations at both sites, these hot spots contributed disproportionately to total emissions. At the CC site, two hot spots had median emissions of 44 and 88 μg N_2O m^{-2} h^{-1} versus a site median of 13 μg N_2O m^{-2} h^{-1}. At the CCF site, three hot spots reached medians of 54, 111, and 149 μg N_2O m^{-2} h^{-1}, far above the site median of 9 μg N_2O m^{-2} h^{-1}. Similar contributions of N_2O hot spots have been reported in other boreal peat soils (Rautakoski et al., 2024). Hot spots in these soils often arise from complex interactions among Ts, Sm, inorganic N, microbial-plant N competition, and physical constraints on N_2O diffusion (Pärn et al., 2018; Voigt et al., 2020). In this study, only the two highest-emission hot spots at the CCF site exhibited slightly elevated soil fertility (Supplementary Fig. S5). Our unbalanced sampling design limited accurate identification of hot spots, which may introduce uncertainty to site-level flux estimates. Therefore, results should be interpreted cautiously but emphasize the need to better account for unpredictable spatial heterogeneity and the substantial role of hot spots in shaping site-level N_2O emissions. Future field campaigns in boreal drained peatland forests should explicitly incorporate spatial heterogeneity in their sampling strategies to improve the accuracy and representativeness of N_2O flux assessments.

4.2.2. Dominance of soil heterogeneity over harvesting in shaping spatial N_2O flux patterns

High spatial variability likely reflects complex interactions of long-term, fine-scale spatial controls. Interestingly, significant positive correlations were found between soil N_2O fluxes and diverse peat nutrient contents (Fig. 8), including K, Cu, and P. Potassium showed the strongest association, as elevated K availability can stimulate microbial activity and influence nitrification and denitrification pathways (Li et al., 2020; Zhang et al., 2022b). Although Cu inhibits microbial activity at high concentrations (Chen et al., 2022; Elrys et al., 2024), our findings align with studies reporting enhanced nitrification at low Cu levels in peat soils (Liimatainen et al., 2018; Matse et al., 2023). Cu concentrations at our site (2.7 and 9.3 mg kg^{-1}) fall within this range, likely supporting microbial activity as a cofactor in key nitrification enzymes such as ammonia monooxygenase (Hooper et al., 1997). In N-rich peatlands, increased P can promote denitrifier activity and microbial O_2 consumption, enhancing denitrification (Liimatainen et al., 2018; Mori et al., 2010; Regina et al., 1996). These findings suggest site-specific nutrient conditions strongly influence spatial N_2O emissions and should be considered when assessing emission potential of peat soils under different harvesting strategies.

Lower CN ratios were also linked to higher fluxes, as they support net N mineralization and increase NH_4^+ and NO_3^- availability (Butterbach-Bahl et al., 2013). However, predictive value declines below ~30 (Supplementary Fig. S5), where variability in N_2O emissions increases (Klemedtsson et al., 2005; Minkkinen et al., 2020). Increased BD and Ts were also associated with higher fluxes, highlighting key mechanisms through which harvesting can influence emissions in boreal drained peatland forests. High BD reduces soil porosity and promotes anoxic conditions, favouring denitrification (Maljanen et al., 2024). Harvesting, especially with heavy machinery, can further increase BD via compaction and peat fibre shrinkage, especially under conditions of increased evaporation and reduced canopy cover (Hooijer et al., 2012). This aligns with previous observations of elevated post-harvest N_2O emissions in logging trails (Korkiakoski et al., 2020). Higher Ts after canopy removal can stimulate microbial activity and N mineralization while accelerating microbial respiration, depleting soil O_2 and enhancing denitrification (Shi et al., 2012; Smith, 1997). Together, these changes suggest that intensive harvesting practices can substantially increase the risk of N_2O emissions by altering key soil physical and thermal properties. Less disruptive harvesting strategies, such as CCF, may help preserve soil structure and microclimate, thereby mitigating post-harvest N_2O emissions.

While spatial soil data mainly represent pre-harvest conditions and fluxes were collected post-harvest, this temporal mismatch limits causal interpretation but confirms that inherent spatial variability remains relevant. Instead, baseline soil heterogeneity may predispose microsites to higher emissions after harvesting, particularly under intensive management. Overall, results highlight the importance of accounting for fine-scale spatial variability when interpreting harvesting effects and scaling emissions from boreal forestry-drained peatlands. Building on this, these forest ecosystems generally exhibit considerable spatial heterogeneity in soil N_2O fluxes (Rautakoski et al., 2024). Our findings align with this observation, yet harvesting increased overall emissions without notably affecting pre-existing spatial variability. Specifically, MC-based measurements showed that the IQR of soil N_2O fluxes remained largely unchanged between pre- and post-harvest conditions in 2020 and 2022, respectively (Fig. 4). This suggests that short-term harvesting-induced changes, such as those in environmental conditions, C inputs, vegetation cover, microbial activity, and nutrient availability, may not be sufficient to immediately override longer-term, more stable controls on soil nitrification and denitrification processes. Consequently, spatial factors, particularly soil fertility, exert a stronger influence than harvesting interventions in controlling the spatial distribution of emissions. Therefore, further studies should clarify the relative contribution of inherent spatial variability to improve predictions of N_2O emissions from forestry-drained boreal peatlands under different harvesting regimes.

4.2.3. Deeper soil profile properties modulate topsoil N_2O fluxes

Our findings indicate that topsoil N_2O fluxes may be more strongly influenced by spatial controlling factors in subsurface soil layers than by

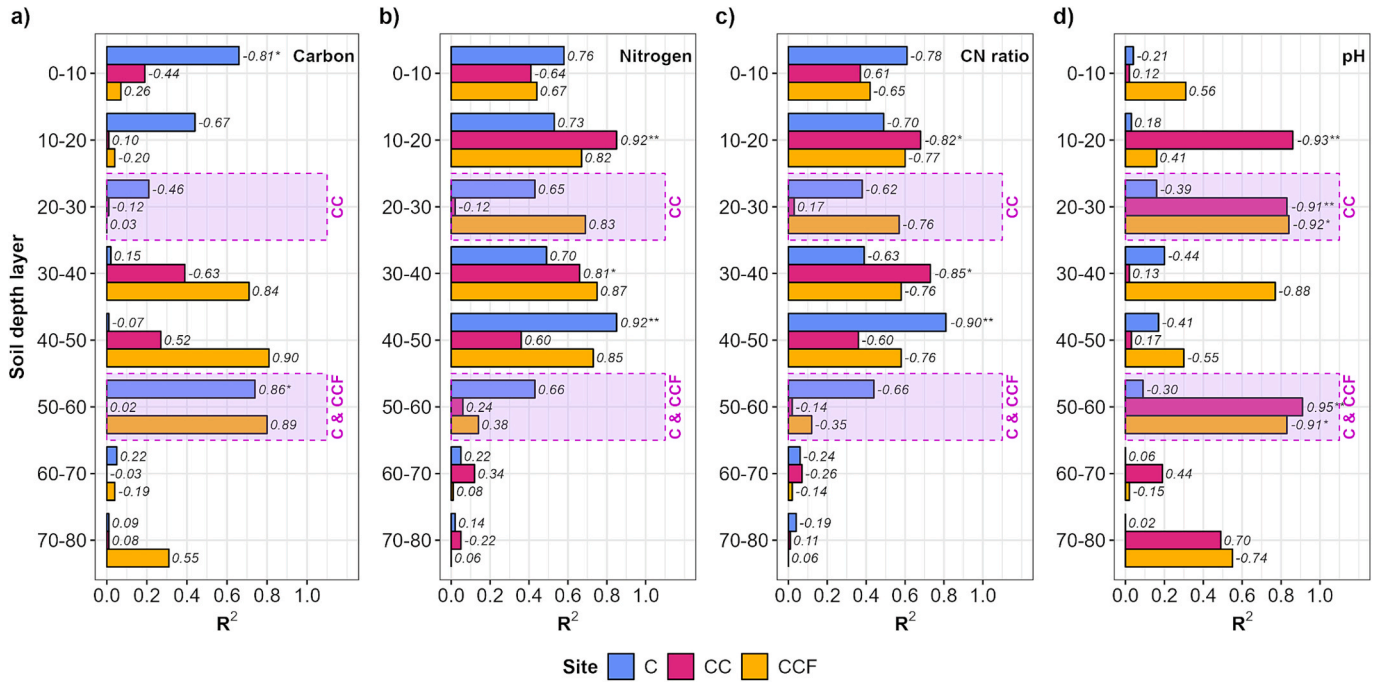

Fig. 9. Deep soil controlling factors of topsoil N_2O fluxes. Panels show correlation analyses between topsoil mean daily N_2O fluxes and a) carbon (%), b) nitrogen (%), c) CN ratio, and d) pH across multiple soil depth layers at the C, CC, and CCF sites. Fluxes are averages from combined MC and AC data during the 2022 growing season. Soil depths include 0–10 cm to 70–80 cm; 80–100 cm layers excluded due to incomplete data. Shaded areas indicate the soil depth layer where the WTL was located during the 2022 growing season at each site (median [IQR]: –58 [41] cm, –29 [12] cm, and –56 [13] cm at the C, CC, and CCF sites, respectively; Supplementary Fig. S7). These WTL values are similar to those measured across all MC and AC sampling locations (Supplementary Fig. S2c). Italicized values indicate Pearson's correlation coefficients; two asterisks for significance ($p < 0.05$), one for marginal ($p < 0.1$), none for non-significant. Sample sizes: $n = 4 + 1$, $4 + 1$, and $4 + 0$ (MC + AC) sampling locations for C, CC, and CCF sites, respectively.

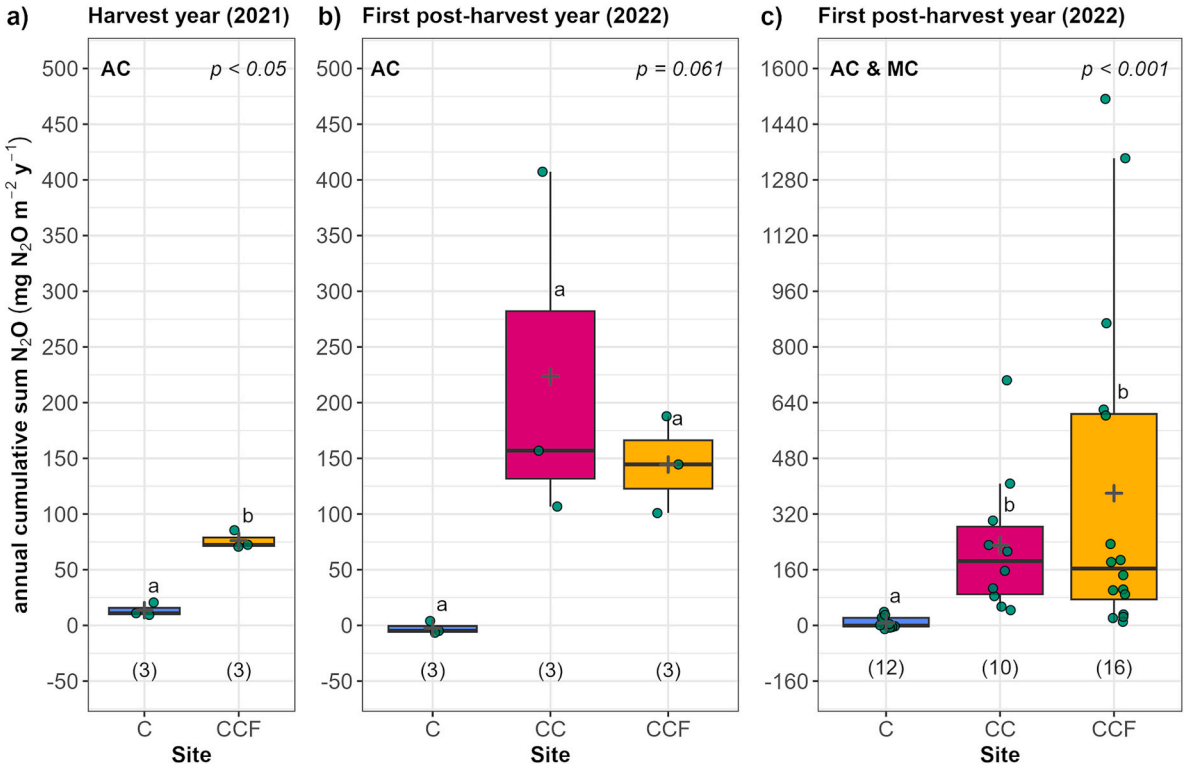

Fig. 10. Annual cumulative soil N_2O fluxes. Panels show annual cumulative sums of N_2O at the C, CC, and CCF sites based on a) AC data during the harvest year (2021), b) AC data during the first post-harvest year (2022), and c) combined AC and MC data during the first post-harvest year (2022). For each panel, the *p*-value is shown for the non-parametric Kruskal–Wallis rank sum test, with different superscript letters indicating significant differences between sites (Dunn-Bonferroni post hoc test, $p < 0.05$). Note that the *y*-axis scales differ between panels a–b) and panel c). Values in parentheses indicate the total number of sampling locations per site.

those in the surface layer (Fig. 8), consistent with previous observations in peat soils (Liimatainen et al., 2018). The upper peat layer is more susceptible to short-term fluctuations in nutrient reservoirs and environmental conditions such as Ts and Sm, leading to greater variability in microbial communities and their associated activities, whereas deeper layers may reflect more stable conditions.

Topsoil N_2O emissions were correlated with peat fertility, reflected in N availability and the CN ratio, in layers above the WTL, with the strongest correlations occurring just above it (Fig. 9). This likely reflects vertical segregation of nitrification and denitrification processes along the soil profile, with nitrification dominating upper layers and denitrification deeper, more anoxic zones (Peltoniemi et al., 2023). It also suggests that seasonal drying-rewetting cycles near the prevailing WTL strongly influence N transformations. Indeed, previous research shows that WTL fluctuations around the saturated–unsaturated interface critically affect soil O_2 availability and redox potential (Rubol et al., 2012), both key regulators of N_2O emissions.

4.3. Short-term effects of contrasting harvesting methods on soil N_2O fluxes

4.3.1. Short-term increase in soil N_2O fluxes after harvesting: Climate benefits of selection harvesting over clear-cutting

Manual chamber-based measurements conducted during June-August showed that both CC and CCF increased median soil N_2O emissions in the first post-harvest year compared to pre-harvest levels, although these increases were not statistically significant (Fig. 4). Considering annual balances, emissions showed a non-significant rise with harvesting intensity, with CC resulting in greater emissions (185 [194] mg N_2O m^{-2} y^{-1}), while CCF exhibited slightly lower emissions (163 [533] mg N_2O m^{-2} y^{-1}) (Fig. 10c). These results are consistent with findings from the Lettosuo experimental site, a nearby forestry-drained peatland located 92 km southwest, where CCF led to substantially lower post-harvest soil N_2O emissions than CC (930 vs. 3700 mg N_2O m^{-2} y^{-1}, respectively; Korkiakoski et al., 2020, Korkiakoski et al., 2019). Differences in emission magnitudes between studies may reflect lower fertility at our site, indicated by a higher average soil CN ratio (30.4 versus 24.4), as well as instrumental, methodological, and/or environmental factors. To improve generalizability of findings across boreal drained peatland forests, future research should cover a broader fertility gradient, from nutrient-rich to nutrient-poor sites, as fertility strongly influences microbial processes and N_2O responses to harvesting. Overall, these findings suggest that transitioning from CC to CCF has the potential to reduce short-term post-harvest soil N_2O emissions, thereby contributing to climate change mitigation in boreal drained peatland forests.

4.3.2. Toward improved N_2O flux estimates: Current limitations and future research directions

Information on CCF impacts on soil N_2O emissions in boreal peatland forests remains limited, with most data coming from only a few recent studies (Korkiakoski et al., 2020; Peltoniemi et al., 2023), reflecting its relatively recent ongoing experimental evaluation in these forest ecosystems (Laudon and Maher Hasselquist, 2023; Nieminen et al., 2018). In contrast, CC has been more extensively studied, mainly via chamber-based measurements (Korkiakoski et al., 2019; Mäkiranta et al., 2012; Tong et al., 2022). However, CC causes extensive soil disturbance and creates a complex mosaic of surface types, complicating accurate chamber-based flux quantification. This may partly explain notably higher emissions reported by eddy covariance at the CC site in 2022 (1829 mg N_2O m^{-2} y^{-1}, Tikkasalo et al., 2025) compared to our chamber-based results. Our sampling covered harvest residues, field-layer vegetation and exposed peat (7.9 %, 11.8 %, and 29.0 % of the CC site), but excluded other surface types such as retained living trees, litter, and dead wood (4.2 %, 19.9 %, and 22.8 %), identified as significant N_2O sources (Tikkasalo et al., 2025). In addition to spatial underrepresentation, discrepancies between methods may reflect the limited temporal resolution in MC measurements, which, even with AC-derived annual estimates, may miss episodic hot moments. Future research should therefore refine sampling strategies and integrate remote sensing technologies, such as satellite or drone imagery, to better classify and upscale chamber-based flux measurements, while increasing sampling frequency across heterogeneous post-clearcut areas in boreal peatland forests.

Regarding WTL management, maintaining continuous tree cover under CCF may better balance timber production and GHG mitigation than CC (Leppä et al., 2020; Nieminen et al., 2018). Optimal WTLs for these climate benefits typically range from 30–40 cm below the peat surface (Ojanen et al., 2013; Sarkkola et al., 2010). At the CCF site, post-harvest WTL remained relatively deep (–58 cm), likely due to effective drainage and only a minor rise (~6 cm; Fig. 3j, Supplementary Fig. S2). This limited shift in WTL, at the lower end of the 4–18 cm range typically reported after selection harvesting (Leppä et al., 2020), is consistent with enhanced transpiration by undergrowth trees and forest-floor vegetation, combined with increased soil evaporation (Leppä et al., 2020). Thus, WTL rise was likely insufficient to markedly reduce N_2O emissions. Therefore, we recommend that future studies explore combining selection harvesting with additional hydrological restoration, such as partial ditch blocking, to raise WTL toward optimal levels and enhance the potential to mitigate N_2O emissions in boreal drained peatland forests.

5. Conclusions

This study provides a comprehensive and timely understanding of the challenges posed by limited research on sustainable harvesting strategies to address the pressing demand to mitigate soil N_2O fluxes in forestry-drained boreal peatlands. It also offers valuable insights into the complex spatio-temporal heterogeneity and underlying factors regulating soil N_2O fluxes in these forest ecosystems.

Our combined manual and automated chamber-based approach, conducted in a nutrient-rich, forestry-drained peatland in southern Finland, revealed substantial temporal variability in soil N_2O fluxes. Ta, precipitation, Sm and WTL emerged as the primary temporal controls. Extensive spatial heterogeneity in emissions was closely linked to soil characteristics, including nutrient concentrations (K, Cu, P, and N), physical properties (BD), and environmental conditions (Ts). At the C site, fluxes remained near neutral throughout the study. Harvesting caused non-significant increases in short-term emissions, but inherent spatial variability played a larger role in shaping their spatial distribution. In the first post-harvest year, emissions showed a non-significant upward trend with harvesting intensity, with clear-cutting resulting in a more pronounced increase and selection harvesting under continuous-cover forestry providing slightly greater mitigation potential. Notably, spatial heterogeneity at the CC site was insufficiently captured by chamber-based measurements compared eddy-covariance estimates, whereas WTL changes were modest at the CCF site. Together, these factors may have limited our ability to detect both higher and lower soil N_2O emissions at the respective sites, thereby constraining the identification of more pronounced differences between harvesting methods.

While further long-term and replicated studies are needed to fully assess post-harvest effects on soil N_2O fluxes, our findings suggest that selection harvesting may more effectively mitigate emissions than clear-cutting in nutrient-rich, forestry-drained boreal peatlands.

CRediT authorship contribution statement

Eduardo Martínez-García: Writing – original draft, Visualization, Software, Methodology, Investigation, Formal analysis, Data curation. **Helena Rautakoski:** Writing – review & editing, Software, Methodology, Investigation, Data curation. **Antti J. Rissanen:** Writing – review & editing, Software, Methodology. **Bartosz Adamczyk:** Writing – review & editing, Data curation. **Jani Anttila:** Writing – review & editing, Data

curation. **Aleksi Lehtonen:** Writing – review & editing, Supervision, Project administration, Funding acquisition, Conceptualization. **Qian Li:** Writing – review & editing, Data curation. **Annalea Lohila:** Writing – review & editing, Funding acquisition, Conceptualization. **Mikko Peltoniemi:** Writing – review & editing, Conceptualization. **Sakari Sarkkola:** Writing – review & editing, Conceptualization. **Boris Ťupek:** Writing – review & editing. **Raisa Mäkipää:** Writing – review & editing, Supervision, Resources, Project administration, Funding acquisition, Conceptualization.

Declaration of competing interest

The authors declare that they have no known competing financial interests or personal relationships that could have appeared to influence the work reported in this paper.

Acknowledgements

This study was funded by the European Union's Horizon 2020 program (HoliSoils, grant n° 101000289), the European Union's LIFE program (LIFE-IP CANEMURE-FINLAND, grant n° LIFE17 IPC/FI/000002), and the Research Council of Finland (FORCLIMATE, grant n° 347794). Authors also acknowledge that this study was conducted within the framework of the UNITE (grant n° 359174) and ACCC (grant n° 337552) Flagships, funded by the Research Council of Finland. We also thank the field and other staff at the Natural Resources Institute Finland (Petri Salovaara) and the Finnish Meteorological Institute (Juuso Rainne, Timo Mäkelä, and Mika Korkiakoski) for their valuable assistance in maintaining and operating equipment and experiments, as well as for collecting field data at the Ränskälänkorpi experimental site.

Code availability

The coding used in this study was developed for visualization and statistical analysis, utilising the specific packages outlined in the 'Statistics' subsection. The Authors may provide the code upon request.

Appendix A. Supplementary data

Supplementary data to this article can be found online at https://doi.org/10.1016/j.geoderma.2025.117648.

Data availability

The data supporting the findings of this study are openly available in the Zenodo digital repository, within the 'HoliSoils community', at https://doi.org/10.5281/zenodo.17853193.

References

Butterbach-Bahl, K., Baggs, E.M., Dannenmann, M., Kiese, R., Zechmeister-Boltenstern, S., 2013. Nitrous oxide emissions from soils: how well do we understand the processes and their controls? Philos. Trans. R. Soc. B Biol. Sci. 368, 20130122. https://doi.org/10.1098/rstb.2013.0122.

Cen, X., Müller, C., Kang, X., Zhou, X., Zhang, J., Yu, G., He, N., 2024. Nitrogen deposition contributed to a global increase in nitrous oxide emissions from forest soils. Commun. Earth Environ. 5, 1–11. https://doi.org/10.1038/s43247-024-01647-6.

Chapuis-Lardy, L., Wrage, N., Metay, A., Chotte, J.-L., Bernoux, M., 2007. Soils, a sink for N_2O? A review. Glob. Change Biol. 13, 1–17. https://doi.org/10.1111/j.1365-2486.2006.01280.x.

Chen, G., Li, J., Han, H., Du, R., Wang, X., 2022. Physiological and molecular mechanisms of plant responses to copper stress. Int. J. Mol. Sci. 23, 12950. https://doi.org/10.3390/ijms232112950.

Cowan, N.J., Famulari, D., Levy, P.E., Anderson, M., Reay, D.S., Skiba, U.M., 2014. Investigating uptake of N_2O in agricultural soils using a high-precision dynamic chamber method. Atmosph. Meas. Tech. 7, 4455–4462. https://doi.org/10.5194/amt-7-4455-2014.

Dyrrdal, A.V., Médus, E., Dobler, A., Hodnebrog, Ø., Arnbjerg-Nielsen, K., Olsson, J., Thomassen, E.D., Lind, P., Gaile, D., Post, P., 2023. Changes in design precipitation over the Nordic-Baltic region as given by convection-permitting climate simulations. Weather Clim. Extrem. 42, 100604. https://doi.org/10.1016/j.wace.2023.100604.

Elrys, A.S., Wen, Y., Qin, X., Chen, Y., Zhu, Q., Eltahawy, A.M., Dan, X., Tang, S., Wu, Y., Zhu, T., Meng, L., Zhang, J., Müller, C., 2024. Initial evidence on the effect of copper on global cropland nitrogen cycling: a meta-analysis. Environ. Int. 184, 108491. https://doi.org/10.1016/j.envint.2024.108491.

Forster, P., Storelvmo, T., Armour, K., Collins, W., Dufresne, J.-L., Frame, D., Lunt, D.J., Mauritsen, T., Palmer, M.D., Watanabe, M., Wild, M., Zhang, H., 2021. The earth's energy budget, climate feedbacks, and climate sensitivity. In: Masson-Delmotte, V., Zhai, P., Pirani, A., Connors, S.L., Péan, C., Berger, S., Caud, N., Chen, Y., Goldfarb, L., Gomis, M.I., Huang, M., Leitzell, K., Lonnoy, E., Matthews, J.B.R., Maycock, T.K., Waterfield, T., Yelekçi, O., Yu, R., Zhou, B. (Eds.), Climate Change 2021: The Physical Science Basis. Contribution of Working Group I to the Sixth Assessment Report of the Intergovernmental Panel on Climate Change. Cambridge University Press, Cambridge, United Kingdom and New York, NY, USA, pp. 923–1054.

Gao, W., Zhao, T., Zhang, Y., Yang, X., Shi, B., Xu, W., Yang, T., Ma, J., Sun, W., 2024. Synergistic effects of precipitation events and long-term N addition on N_2O emissions in a temperate meadow steppe, Northeast China. Agric. For. Meteorol. 345, 109860. https://doi.org/10.1016/j.agrformet.2023.109860.

Giles, M.E., Morley, N.J., Baggs, E.M., Daniell, T.J., 2012. Soil nitrate reducing processes – drivers, mechanisms for spatial variation, and significance for nitrous oxide production. Front. Microbiol. 3. https://doi.org/10.3389/fmicb.2012.00407.

Härkönen, L.H., Lepistö, A., Sarkkola, S., Kortelainen, P., Räike, A., 2023. Reviewing peatland forestry: Implications and mitigation measures for freshwater ecosystem browning. For. Ecol. Manag. 531, 120776. https://doi.org/10.1016/j.foreco.2023.120776.

He, W., Mäkiranta, P., Straková, P., Ojanen, P., Penttilä, T., Bhuiyan, R., Minkkinen, K., Laiho, R., 2023. Fine-root production in boreal peatland forests: Effects of stand and environmental factors. For. Ecol. Manag. 550, 121503. https://doi.org/10.1016/j.foreco.2023.121503.

Helbig, M., Waddington, J.M., Alekseychik, P., Amiro, B.D., Aurela, M., Barr, A.G., Black, T.A., Blanken, P.D., Carey, S.K., Chen, J., Chi, J., Desai, A.R., Dunn, A., Euskirchen, E.S., Flanagan, L.B., Forbrich, I., Friborg, T., Grelle, A., Harder, S., Heliasz, M., Humphreys, E.R., Ikawa, H., Isabelle, P.-E., Iwata, H., Jassal, R., Korkiakoski, M., Kurbatova, J., Kutzbach, L., Lindroth, A., Löfvenius, M.O., Lohila, A., Mammarella, I., Marsh, P., Maximov, T., Melton, J.R., Moore, P.A., Nadeau, D.F., Nicholls, E.M., Nilsson, M.B., Ohta, T., Peichl, M., Petrone, R.M., Petrov, R., Prokushkin, A., Quinton, W.L., Reed, D.E., Roulet, N.T., Runkle, B.R.K., Sonnentag, O., Strachan, I.B., Taillardat, P., Tuittila, E.-S., Tuovinen, J.-P., Turner, J., Ueyama, M., Varlagin, A., Wilmking, M., Wofsy, S.C., Zyrianov, V., 2020. Increasing contribution of peatlands to boreal evapotranspiration in a warming climate. Nat. Clim. Chang. 10, 555–560. https://doi.org/10.1038/s41558-020-0763-7.

Hooijer, A., Page, S., Jauhiainen, J., Lee, W.A., Lu, X.X., Idris, A., Anshari, G., 2012. Subsidence and carbon loss in drained tropical peatlands. Biogeosciences 9, 1053–1071. https://doi.org/10.5194/bg-9-1053-2012.

Hooper, A.B., Vannelli, T., Bergmann, D.J., Arciero, D.M., 1997. Enzymology of the oxidation of ammonia to nitrite by bacteria. Antonie Van Leeuwenhoek 71, 59–67. https://doi.org/10.1023/A:1000133919203.

Klemedtsson, L., Von Arnold, K., Weslien, P., Gundersen, P., 2005. Soil CN ratio as a scalar parameter to predict nitrous oxide emissions. Glob. Chang. Biol. 11, 1142–1147. https://doi.org/10.1111/j.1365-2486.2005.00973.x.

Könönen, M., Jauhiainen, J., Laiho, R., Kusin, K., Vasander, H., 2015. Physical and chemical properties of tropical peat under stabilised land uses. Mires Peat 16, 1–13.

Korkiakoski, M., Ojanen, P., Penttilä, T., Minkkinen, K., Sarkkola, S., Rainne, J., Laurila, T., Lohila, A., 2020. Impact of partial harvest on CH_4 and N_2O balances of a drained boreal peatland forest. Agric. For. Meteorol. 295, 108168. https://doi.org/10.1016/j.agrformet.2020.108168.

Korkiakoski, M., Tuovinen, J.-P., Aurela, M., Koskinen, M., Minkkinen, K., Ojanen, P., Penttilä, T., Rainne, J., Laurila, T., Lohila, A., 2017. Methane exchange at the peatland forest floor – automatic chamber system exposes the dynamics of small fluxes. Biogeosciences 14, 1947–1967. https://doi.org/10.5194/bg-14-1947-2017.

Korkiakoski, M., Tuovinen, J.-P., Penttilä, T., Sarkkola, S., Ojanen, P., Minkkinen, K., Rainne, J., Laurila, T., Lohila, A., 2019. Greenhouse gas and energy fluxes in a boreal peatland forest after clear-cutting. Biogeosciences 16, 3703–3723. https://doi.org/10.5194/bg-16-3703-2019.

Koskinen, M., Minkkinen, K., Ojanen, P., Kämäräinen, M., Laurila, T., Lohila, A., 2014. Measurements of CO_2 exchange with an automated chamber system throughout the year: challenges in measuring night-time respiration on porous peat soil. Biogeosciences 11, 347–363. https://doi.org/10.5194/bg-11-347-2014.

Kuuluvainen, T., Tahvonen, O., Aakala, T., 2012. Even-aged and uneven-aged forest management in boreal Fennoscandia: a review. Ambio 41, 720–737. https://doi.org/10.1007/s13280-012-0289-y.

Laine, A.M., Ojanen, P., Lindroos, T., Koponen, K., Maanavilja, L., Lampela, M., Turunen, J., Minkkinen, K., Tolvanen, A., 2024. Climate change mitigation potential of restoration of boreal peatlands drained for forestry can be adjusted by site selection and restoration measures. Restor. Ecol. 32, e14213. https://doi.org/10.1111/rec.14213.

Laine, J., Vasander, H., Hotanen, J.-P., Nousiainen, H., Saarinen, M., Penttilä, T., 2012. Suotyypit ja turvekankaat – opas kasvupaikkojen tunnistamiseen. Metsäkustannus Oy Hämeenlinna.

Laudon, H., Maher Hasselquist, E., 2023. Applying continuous-cover forestry on drained boreal peatlands; water regulation, biodiversity, climate benefits and remaining uncertainties. Trees For. People 11, 100363. https://doi.org/10.1016/j.tfp.2022.100363.

Lehtonen, A., Eyvindson, K., Härkönen, K., Leppä, K., Salmivaara, A., Peltoniemi, M., Salminen, O., Sarkkola, S., Launiainen, S., Ojanen, P., Räty, M., Mäkipää, R., 2023. Potential of continuous cover forestry on drained peatlands to increase the carbon sink in Finland. Sci. Rep. 13, 15510. https://doi.org/10.1038/s41598-023-42315-7.

Lepilin, D., 2023. Impacts of thinning activities on boreal peatland forests. Diss. For. 33.

Lepilin, D., Laurén, A., Uusitalo, J., Tuittila, E.-S., 2019. Soil deformation and its recovery in logging trails of drained boreal peatlands. Can. J. For. Res. 49, 743–751. https://doi.org/10.1139/cjfr-2018-0385.

Leppä, K., Korkiakoski, M., Nieminen, M., Laiho, R., Hotanen, J.-P., Kieloaho, A.-J., Korpela, L., Laurila, T., Lohila, A., Minkkinen, K., Mäkipää, R., Ojanen, P., Pearson, M., Penttilä, T., Tuovinen, J.-P., Launiainen, S., 2020. Vegetation controls of water and energy balance of a drained peatland forest: responses to alternative harvesting practices. Agric. For. Meteorol. 295, 108198. https://doi.org/10.1016/j.agrformet.2020.108198.

Li, Z., Xia, S., Zhang, R., Zhang, R., Chen, F., Liu, Y., 2020. N_2O emissions and product ratios of nitrification and denitrification are altered by K fertilizer in acidic agricultural soils. Environ. Pollut. 265, 115065. https://doi.org/10.1016/j.envpol.2020.115065.

Liao, J., Zheng, W., Liao, Q., Lu, S., 2024. Global latitudinal patterns in forest ecosystem nitrous oxide emissions are related to hydroclimate. Npj Clim. Atmosph. Sci. 7, 1–10. https://doi.org/10.1038/s41612-024-00737-8.

Liimatainen, M., Voigt;, C., Martikainen, P.J., Hytönen, J., Regina, K., Óskarsson, H., Maljanen, M., 2018. Factors controlling nitrous oxide emissions from managed northern peat soils with low carbon to nitrogen ratio. Soil Biol. Biochem. 122, 186–195. https://doi.org/10.1016/j.soilbio.2018.04.006.

Mäkipää, R., Abramoff, R., Adamczyk, B., Baldy, V., Biryol, C., Bosela, M., Casals, P., Curiel Yuste, J., Dondini, M., Filipek, S., Garcia-Pausas, J., Gros, R., Gömöryová, E., Hashimoto, S., Hassegawa, M., Immonen, P., Laiho, R., Li, H., Li, Q., Luyssaert, S., Menival, C., Mori, T., Naudts, K., Santonja, M., Smolander, A., Toriyama, J., Tupek, B., Ubeda, X., Johannes Verkerk, P., Lehtonen, A., 2023. How does management affect soil C sequestration and greenhouse gas fluxes in boreal and temperate forests? – a review. For. Ecol. Manag. 529, 120637. https://doi.org/10.1016/j.foreco.2022.120637.

Mäkiranta, P., Laiho, R., Penttilä, T., Minkkinen, K., 2012. The impact of logging residue on soil GHG fluxes in a drained peatland forest. Soil Biol. Biochem. 48, 1–9. https://doi.org/10.1016/j.soilbio.2012.01.005.

Maljanen, M., Liikanen, A., Silvola, J., Martikainen, P.J., 2003. Nitrous oxide emissions from boreal organic soil under different land-use. Soil Biol. Biochem. 35, 689–700. https://doi.org/10.1016/S0038-0717(03)00085-3.

Maljanen, M., Zheng, Y., Pääkkönen, M., Voigt;, C., Louhisuo, A., Virkajärvi, P., 2024. Phosphorus - a key element determining nitrous oxide emissions from boreal cultivated peat soil. Soil Biol. Biochem. 195, 109483. https://doi.org/10.1016/j.soilbio.2024.109483.

Matse, D.T., Jeyakumar, P., Bishop, P., Anderson, C.W.N., 2023. Copper induces nitrification by ammonia-oxidizing bacteria and archaea in pastoral soils. J. Environ. Qual. 52, 49–63. https://doi.org/10.1002/jeq2.20440.

Minkkinen, K., Ojanen, P., Koskinen, M., Penttilä, T., 2020. Nitrous oxide emissions of undrained, forestry-drained, and rewetted boreal peatlands. For. Ecol. Manag. 478, 118494. https://doi.org/10.1016/j.foreco.2020.118494.

Mori, T., Ohta, S., Ishizuka, S., Konda, R., Wicaksono, A., Heriyanto, J., Hardjono, A., 2010. Effects of phosphorus addition on N_2O and NO emissions from soils of an Acacia mangium plantation. Soil Sci. Plant Nutr. 56, 782–788. https://doi.org/10.1111/j.1747-0765.2010.00501.x.

Nieminen, M., Hökkä, H., Laiho, R., Juutinen, A., Ahtikoski, A., Pearson, M., Kojola, S., Sarkkola, S., Launiainen, S., Valkonen, S., Penttilä, T., Lohila, A., Saarinen, M., Haahti, K., Mäkipää, R., Miettinen, J., Ollikainen, M., 2018. Could continuous cover forestry be an economically and environmentally feasible management option on drained boreal peatlands? For. Ecol. Manag. 424, 78–84. https://doi.org/10.1016/j.foreco.2018.04.046.

Ojanen, P., Minkkinen, K., Alm, J., Penttilä, T., 2010. Soil–atmosphere CO_2, CH_4 and N_2O fluxes in boreal forestry-drained peatlands. For. Ecol. Manag. 260, 411–421. https://doi.org/10.1016/j.foreco.2010.04.036.

Ojanen, P., Minkkinen, K., Penttilä, T., 2013. The current greenhouse gas impact of forestry-drained boreal peatlands. For. Ecol. Manag. 289, 201–208. https://doi.org/10.1016/j.foreco.2012.10.008.

Oktarita, S., Hergoualc'h, K., Anwar, S., Verchot, L.V., 2017. Substantial N_2O emissions from peat decomposition and N fertilization in an oil palm plantation exacerbated by hotspots. Environ. Res. Lett. 12, 104007. https://doi.org/10.1088/1748-9326/aa80f1.

Pan, Y., Birdsey, R.A., Fang, J., Houghton, R., Kauppi, P.E., Kurz, W.A., Phillips, O.L., Shvidenko, A., Lewis, S.L., Canadell, J.G., Ciais, P., Jackson, R.B., Pacala, S.W., McGuire, A.D., Piao, S., Rautiainen, A., Sitch, S., Hayes, D., 2011. A large and persistent carbon sink in the world's forests. Science 333, 988–993. https://doi.org/10.1126/science.1201609.

Pandey, C.B., Kumar, U., Kaviraj, M., Minick, K.J., Mishra, A.K., Singh, J.S., 2020. DNRA: a short-circuit in biological N-cycling to conserve nitrogen in terrestrial ecosystems. Sci. Total Environ. 738, 139710. https://doi.org/10.1016/j.scitotenv.2020.139710.

Pärn, J., Verhoeven, J.T.A., Butterbach-Bahl, K., Dise, N.B., Ullah, S., Aasa, A., Egorov, S., Espenberg, M., Järveoja, J., Jauhiainen, J., Kasak, K., Klemedtsson, L., Kull, A., Laggoun-Défarge, F., Lapshina, E.D., Lohila, A., Lõhmus, K., Maddison, M., Mitsch, W.J., Müller, C., Niinemets, Ü., Osborne, B., Pae, T., Salm, J.-O., Sgouridis, F., Sohar, K., Soosaar, K., Storey, K., Teemusk, A., Tenywa, M.M., Tournebize, J., Truu, J., Veber, G., Villa, J.A., Zaw, S.S., Mander, Ü., 2018. Nitrogen-rich organic soils under warm well-drained conditions are global nitrous oxide emission hotspots. Nat. Commun. 9, 1135. https://doi.org/10.1038/s41467-018-03540-1.

Peltoniemi, M., Li, Q., Turunen, P., Tupek, B., Mäkiranta, P., Leppä, K., Müller, M., Rissanen, A.J., Laiho, R., Anttila, J., Jauhiainen, J., Koskinen, M., Lehtonen, A., Ojanen, P., Pihlatie, M., Sarkkola, S., Vainio, E., Mäkipää, R., 2023. Soil GHG dynamics after water level rise – Impacts of selection harvesting in peatland forests. Sci. Total Environ. 901, 165421. https://doi.org/10.1016/j.scitotenv.2023.165421.

Pihlatie, M.K., Kiese, R., Brüggemann, N., Butterbach-Bahl, K., Kieloaho, A.-J., Laurila, T., Lohila, A., Mammarella, I., Minkkinen, K., Penttilä, T., Schönborn, J., Vesala, T., 2010. Greenhouse gas fluxes in a drained peatland forest during spring frost-thaw event. Biogeosciences 7, 1715–1727. https://doi.org/10.5194/bg-7-1715-2010.

Rautakoski, H., Korkiakoski, M., Mäkelä, J., Koskinen, M., Minkkinen, K., Aurela, M., Ojanen, P., Lohila, A., 2024. Exploring temporal and spatial variation of nitrous oxide flux using several years of peatland forest automatic chamber data. Biogeosciences 21, 1867–1886. https://doi.org/10.5194/bg-21-1867-2024.

Rautio, P., Routa, J., Huuskonen, S., Holmström, E., Cedergren, J., Kuehne, C. (Eds.), 2025. Continuous Cover Forestry in Boreal Nordic Countries, Managing Forest Ecosystems. Springer Cham. https://doi.org/10.1007/978-3-031-70484-0.

Ravishankara, A.R., Daniel, J.S., Portmann, R.W., 2009. Nitrous oxide (N_2O): the dominant ozone-depleting substance emitted in the 21st century. Science 326, 123–125. https://doi.org/10.1126/science.1176985.

Regina, K., Nykänen, H., Maljanen, M., Silvola, J., Martikainen, P.J., 1998. Emissions of N_2O and NO and net nitrogen mineralization in a boreal forested peatland treated with different nitrogen compounds. Can. J. For. Res. 28, 132–140. https://doi.org/10.1139/x97-198.

Regina, K., Nykänen, H., Silvola, J., Martikainen, P.J., 1996. Fluxes of nitrous oxide from boreal peatlands as affected by peatland type, water table level and nitrification capacity. Biogeochemistry 35, 401–418. https://doi.org/10.1007/BF02183033.

Rubol, S., Silver, W.L., Bellin, A., 2012. Hydrologic control on redox and nitrogen dynamics in a peatland soil. Sci. Total Environ. 432, 37–46. https://doi.org/10.1016/j.scitotenv.2012.05.073.

Sarkkola, S., Hökkä, H., Koivusalo, H., Nieminen, M., Ahti, E., Päivänen, J., Laine, J., 2010. Role of tree stand evapotranspiration in maintaining satisfactory drainage conditions in drained peatlands. Can. J. For. Res. 40, 1485–1496. https://doi.org/10.1139/X10-084.

Schelker, J., Kuglerová, L., Eklöf, K., Bishop, K., Laudon, H., 2013. Hydrological effects of clear-cutting in a boreal forest – Snowpack dynamics, snowmelt and streamflow responses. J. Hydrol. 484, 105–114. https://doi.org/10.1016/j.jhydrol.2013.01.015.

Shi, F., Chen, H., Chen, H., Wu, Y., Wu, N., 2012. The combined effects of warming and drying suppress CO_2 and N_2O emission rates in an alpine meadow of the eastern Tibetan Plateau. Ecol. Res. 27, 725–733. https://doi.org/10.1007/s11284-012-0950-8.

Si, Y., Zhu, Y., Sanders, I., Kinkel, D.B., Purdy, K.J., Trimmer, M., 2023. Direct biological fixation provides a freshwater sink for N_2O. Nat. Commun. 14, 6775. https://doi.org/10.1038/s41467-023-42481-2.

Sikström, U., Hökkä, H., 2015. Interactions between soil water conditions and forest stands in boreal forests with implications for ditch network maintenance. Silva Fenn. 50. https://doi.org/10.14214/sf.1416.

Smith, K., 1997. The potential for feedback effects induced by global warming on emissions of nitrous oxide by soils. Glob. Chang. Biol. 3, 327–338. https://doi.org/10.1046/j.1365-2486.1997.00100.x.

Stuchiner, E.R., Xu, J., Eddy, W.C., DeLucia, E.H., Yang, W.H., 2025. Hot or not? An evaluation of methods for identifying hot moments of nitrous oxide emissions from soils. J. Geophys. Res. Biogeosci. 130, e2024JG008138. https://doi.org/10.1029/2024JG008138.

Tian, H., Pan, N., Thompson, R.L., Canadell, J.G., Suntharalingam, P., Regnier, P., Davidson, E.A., Prather, M., Ciais, P., Muntean, M., Pan, S., Winiwarter, W., Zaehle, S., Zhou, F., Jackson, R.B., Bange, H.W., Berthet, S., Bian, Z., Bianchi, D., Bouwman, A.F., Buitenhuis, E.T., Dutton, G., Hu, M., Ito, A., Jain, A.K., Jeltsch-Thömmes, A., Joos, F., Kou-Giesbrecht, S., Krummel, P.B., Lan, X., Landolfi, A., Lauerwald, R., Li, Y., Lu, C., Maavara, T., Manizza, M., Millet, D.B., Mühle, J., Patra, P.K., Peters, G.P., Qin, X., Raymond, P., Resplandy, L., Rosentreter, J.A., Shi, H., Sun, Q., Tonina, D., Tubiello, F.N., van der Werf, G.R., Vuichard, N., Wang, J., Wells, K.C., Western, L.M., Wilson, C., Yang, J., Yao, Y., You, Y., Zhu, Q., 2024. Global nitrous oxide budget (1980–2020). Earth Syst. Sci. Data 16, 2543–2604. https://doi.org/10.5194/essd-16-2543-2024.

Tikkasalo, O.-P., Peltola, O., Alekseychik, P., Heikkinen, J., Launiainen, S., Lehtonen, A., Li, Q., Martínez-García, E., Peltoniemi, M., Salovaara, P., Tuominen, V., Mäkipää, R., 2025. Eddy-covariance fluxes of CO_2, CH_4 and N_2O in a drained peatland forest after clear-cutting. Biogeosciences 22, 1277–1300. https://doi.org/10.5194/bg-22-1277-2025.

Tong, C.H.M., Nilsson, M.B., Sikström, U., Ring, E., Drott, A., Eklöf, K., Futter, M.N., Peacock, M., Segersten, J., Peichl, M., 2022. Initial effects of post-harvest ditch cleaning on greenhouse gas fluxes in a hemiboreal peatland forest. Geoderma 426, 116055. https://doi.org/10.1016/j.geoderma.2022.116055.

UNEP, 2022. Global Peatlands Assessment – the State of the World's Peatlands: evidence for action toward the conservation, restoration, and sustainable management of peatlands. Main Report. Global Peatlands Initiative. United Nations Environment Programme, Nairobi.

Van Rossum, G., Drake, F.L., 2009. Python 3 Reference Manual. CreateSpace, Scotts Valley, CA.

Voigt;, C., Marushchak, M.E., Abbott, B.W., Biasi, C., Elberling, B., Siciliano, S.D., Sonnentag, O., Stewart, K.J., Yang, Y., Martikainen, P.J., 2020. Nitrous oxide emissions from permafrost-affected soils. Nat. Rev. Earth Environ. 1, 420–434. https://doi.org/10.1038/s43017-020-0063-9.

Wagner-Riddle, C., Baggs, E.M., Clough, T.J., Fuchs, K., Petersen, S.O., 2020. Mitigation of nitrous oxide emissions in the context of nitrogen loss reduction from

agroecosystems: managing hot spots and hot moments. Climate Change, Reactive Nitrogen, Food Security and Sustainable Agriculture Curr. Opin. Environ. Sustain. 47, 46–53. https://doi.org/10.1016/j.cosust.2020.08.002.

Wen, Y., Chen, Z., Dannenmann, M., Carminati, A., Willibald, G., Kiese, R., Wolf, B., Veldkamp, E., Butterbach-Bahl, K., Corre, M.D., 2016. Disentangling gross N_2O production and consumption in soil. Sci. Rep. 6, 36517. https://doi.org/10.1038/srep36517.

Wilson, S.J., Song, B., Phillips, R.L., 2021. Determining chemical factors controlling abiotic codenitrification. ACS Earth Space Chem. 5, 186–196. https://doi.org/10.1021/acsearthspacechem.0c00225.

Zhang, H., Tang, C., Berninger, F., Bai, S., Wang, H., Wang, Y., 2022a. Intensive forest harvest increases N_2O emission from soil: a meta-analysis. Soil Biol. Biochem. 172, 108712. https://doi.org/10.1016/j.soilbio.2022.108712.

Zhang, Y.-B., Liu, F., Wang, J.-T., Hu, H.-W., He, J.-Z., Zhang, L.-M., 2022b. Effect of straw incorporation and nitrification inhibitor on nitrous oxide emission in three cropland soils. J. Sustain. Agric. Environ. 1, 132–141. https://doi.org/10.1002/sae2.12013.